INTERNATIONAL JOURNAL FOR NUMERICAL METHODS IN FLUIDS, VOL. 23, 1163–1195 (1996)

NESTED GRID METHODS FOR AN OCEAN MODEL: A COMPARATIVE STUDY

MARC LAUGIER

Centre d'Océanologie de Marseille, Campus de Luminy, Case 901, UMR 41, CNRS, Université Aix-Marseille II, F-13288 Marseille Cedex 9, France

PHILIPPE ANGOT

Institut de Recherche sur les Phénomènes Hors Equilibre, UMR 138, CNRS, Universités Aix-Marseille I et II, 12 Avenue du Général Leclerc, F-13003 Marseille, France

AND

LAURENT MORTIER

Cabinet d'Etudes Techniques Industrielles et d'Innovations Scientifiques, 24 Boulevard Paul Vaillant-Couturier, F-94200 Ivry sur Seine, Paris, France

SUMMARY

In this paper a comparison is carried out between three correction methods for multigrid local mesh refinement in oceanic applications: FIC, LDC and the direct method (DM) proposed by Spall and Holland. This study is based on a nested primitive equation model developed by Laugier on the basis of the code OPA (LODYC). The external barotropic problem is solved using any of the three local grid correction algorithms yielding an interactive nested grid model. The non-linear elliptic equation for the barotropic streamfunction tendency is solved on two nested grids, called the global and the zoom grid, that interact between themselves. The zoom grid is entirely embedded within the global domain with a horizontal grid step ratio of 3:1. The computation on the global grid supplies the boundary conditions for the zoom grid region and the fine grid fields are used to correct the global coarse solution. The three local correction methods are tested on two problems relevant to oceanic circulation phenomena proposed by Spall and Holland: a barotropic modon and an anticyclonic vortex. The results show that the nesting technique is a very efficient way to solve these problems in terms of a gain in precision compared with the required CPU time. The two-domain model with local mesh refinement allows one both to manage effectively the open boundary conditions for the local grid and to correct the global solution thanks to the zoom solution. In the case of the modon propagation the three local correction methods provide approximately the same results. For the baroclinic vortex it appears that the two iterative methods are more efficient than the direct one.

KEY WORDS: ocean circulation model; primitive equations; interactive nested grid model; multidomain methods; multigrid local mesh refinement; local grid correction

1. INTRODUCTION

For oceanic circulation problems, in order to increase the horizontal resolution in a subregion without incurring the computational expense of high resolution over the entire domain, a nested primitive

CCC 0271–2091/96/111163–33

Received June 1995
Revised February 1996

equation model has been developed.[1,2] Moreover, computer resources may be wasted in regions where the flow is sufficiently smooth. Oceanic phenomena cover a disparate range of spatial scales from turbulence, eddies and fronts to planetary waves. Therefore a single mesh size could be insufficient to modelize these processes correctly without exceeding computer limitations. The nested grid technique is a very efficient way to overcome these difficulties. This technique has been widely used in meteorology[3–5] and more recently in oceanography, for which some examples of applications can be found in References 6 and 7. The drawback of this technique is the great number of parameters or the generation of new problems—grid interaction, computational efficiency and conservation properties—compared with a classical technique with a single expandable grid. In the present study we have chosen to compare three local grid correction methods allowing a multigrid mesh refinement within an interactive nested grid model. The embedded model, which uses a fine grid (FG) and a coarse grid (CG) that interact between themselves, is built from an ocean circulation model[8] based on the formulation proposed by Bryan.[9] This formulation of the primitive equations using the barotropic streamfunction involves the resolution of an elliptic problem coupled with a parabolic problem corresponding to the baroclinic part. We propose here to compare the three local grid correction methods for the implicit resolution of the elliptic problem, the explicit part being solved as described in a previous study.[1,2] Usually in the nested model the barotropic streamfunction equation is solved on two grids by a simple direct method (DM).[6,7] We propose here to compare this direct method with the two iterative methods FIC[10,11] and LDC.[12,13] These local grid iterative correction methods were originally developed for elliptic problems and have not yet been tested on the three-dimensional primitive equation model, though the FIC method has been validated in a two-dimensional case.[14,15] In Section 2 of this study we present the basic equation model and the Poisson-like equation for the barotropic streamfunction tendency which is to be solved on two nested domains. The general methodology and the three local grid correction algorithms used for the resolution of the non-linear elliptic problem for the streamfunction are described in a unified presentation in Section 3. The two test problems and the numerical results are finally discussed in Section 4.

2. BASIC MODEL

2.1. Physical model

The embedded model described in this paper uses, on both the local and global grids, the primitive Reynolds-averaged Navier–Stokes equations for a stratified, incompressible fluid, assuming that the hydrostatic and Boussinesq approximations are valid.

In any orthogonal co-ordinate system (x, y, z) the conservation of the momentum of a fluid element yields

$$\partial_t \mathbf{U}_h + (\mathbf{k} \cdot \nabla \times \mathbf{U}_h + f)\mathbf{k} \times \mathbf{U}_h + w\partial_z \mathbf{U}_h + \frac{1}{\rho_0}\nabla[p + \tfrac{1}{2}\rho_0(\mathbf{U}_h)^2] = \mathscr{F}^{\mathbf{U}}(\mathbf{U}_h), \tag{1}$$

where $\mathbf{U}_h = (u, v, 0)$ and w are the horizontal and vertical velocity components respectively, f is the Coriolis parameter ($f = 2\boldsymbol{\Omega} \cdot \mathbf{k}$, where $\boldsymbol{\Omega}$ is the Earth's angular velocity vector and $\mathbf{k}$ is the vertical unit vector oriented along the vertically ascendent direction z), ρ_0 is a reference density and p is the pressure.

For a fluid without internal sources or sinks the conservation of heat may be written as

$$\partial_t T + \nabla \cdot (T\mathbf{U}_h) + \partial_z(Tw) = \mathscr{F}^T(T), \tag{2}$$

where T is the potential temperature.

The hydrostatic assumption gives, according to the Boussinesq assumption,

$$\partial_z p + \rho g = 0, \tag{3}$$

where g is the gravitational acceleration.

The continuity equation is

$$\nabla \cdot \mathbf{U}_h + \partial_z w = 0. \tag{4}$$

An equation of state is used to calculate the *in situ* density ρ from the temperature. In the present study this equation has been simplified by not including the effects of salinity, so that

$$\rho = \rho(T). \tag{5}$$

For the purpose of simplification the salinity transport diffusion equation, analogous to the temperature equation (2), will not be considered here.

The turbulence closure hypothesis consists of the specification of the turbulence tensors (which represent on the large scale the effect of small-scale dynamics and thermodynamics) in terms of only large-scale dynamic and thermodynamic features.

We chose a classical turbulence model where the viscous and thermal diffusion terms $\mathscr{F}^{\mathbf{U}}(\mathbf{U}_h)$ and $\mathscr{F}^{T}(T)$ correspond to zero-order Reynolds tensor modelling:

$$\mathscr{F}^{\mathbf{U}}(\mathbf{U}_h) = v_{th}[\nabla(\nabla \cdot \mathbf{U}_h) - \nabla \times (\nabla \times \mathbf{U}_h)] + \partial_z(v_{tz}\partial_z \mathbf{U}_h) = v_{th}\Delta \mathbf{U}_h + \partial_z(v_{tz}\partial_z \mathbf{U}_h), \tag{6}$$

$$\mathscr{F}^{T}(T) = \kappa_{th}\Delta_h T + \partial_z(\kappa_{tz}\partial_z T), \tag{7}$$

where v_{th}, v_{tz} and κ_{th}, κ_{tz} are the viscous and diffusive turbulence coefficients respectively. In order to simplify the present study, these coefficients are chosen constant (see Tables I and II), but other turbulence closure models could be used[8] if necessary.

2.2. *Numerical methodology*

2.2.1. Procedure for filtering external gravity waves. The procedure used to solve the momentum equation on the local and global grids is the method first introduced by Bryan.[9] The rigid lid approximation is made, i.e. $w(z = 0) = 0$, which allows us to filter the external gravity waves without suppressing the pressure variation at the ocean surface. Vertical integration of the continuity equation (4) and the hydrostatic equation (3) gives the vertical velocity and pressure, the latter being decomposed into surface and hydrostatic pressure:

$$w(x, y, z, t) = \int_z^0 \nabla \cdot \mathbf{U}_h \mathrm{d}\zeta, \tag{8}$$

$$p(x, y, z, t) = p_s(x, y, t) + p_H(x, y, z, t), \quad \text{with} \quad p_H = \int_z^0 \rho g \mathrm{d}\zeta. \tag{9}$$

If we assume that the vertical velocity at the surface is equal to zero, then, with the help of the continuity equation (4) integrated between the bottom and the ocean surface, together with the kinematic condition at the bottom, i.e. $w(z = -\mathscr{H}) = -\mathbf{U}_h \cdot \nabla\mathscr{H}$, it is easy to show that the external barotropic mode corresponding to the vertically integrated horizontal velocities can be derived from a stream function Ψ:

$$\bar{\mathbf{U}}_h = \frac{1}{\mathscr{H}} \mathbf{k} \times \nabla\Psi, \quad \text{where } \bar{\mathbf{U}}_h = \frac{1}{\mathscr{H}} \int_{-\mathscr{H}}^0 \mathbf{U}_h \mathrm{d}z. \tag{10}$$

The surface pressure is eliminated from the equations by decomposing the horizontal velocity field into the external mode and the internal mode describing the baroclinic deviations from the vertically averaged flow:

$$\hat{\mathbf{U}}_h(x, y, z, t) = \mathbf{U}_h(x, y, z, t) - \bar{\mathbf{U}}_h(x, y, t). \tag{11}$$

Since the surface pressure gradient ∇p_s does not depend on z, equation (1) can be written as

$$\partial_t \bar{\mathbf{U}}_h = \bar{\mathbf{M}}_h - \frac{1}{\rho_0} \nabla p_s, \tag{12}$$

$$\partial_t \hat{\mathbf{U}}_h = \mathbf{M}_h - \bar{\mathbf{M}}_h, \tag{13}$$

where

$$\bar{\mathbf{M}}_h(x, y, t) = \frac{1}{\mathscr{H}} \int_{-\mathscr{H}}^{0} \mathbf{M}_h dz, \tag{14}$$

$$\mathbf{M}_h = (M_u, M_v, 0) = -(\mathbf{k} \cdot \nabla \times \mathbf{U}_h + f)\mathbf{k} \times \mathbf{U}_h - w\partial_z \mathbf{U}_h - \frac{1}{\rho_0} \nabla[p_H + \tfrac{1}{2}\rho_0 (\mathbf{U}_h)^2] + \mathscr{F}^{\mathbf{U}}(\mathbf{U}_h). \tag{15}$$

Then we take the horizontal curl, i.e. the operator $\mathbf{k} \cdot \nabla \times$, of equation (12) to obtain a prognostic equation for the tendency of the barotropic streamfunction Ψ_t:

$$\mathbf{k} \cdot \nabla \times \left(\frac{1}{\mathscr{H}} \mathbf{k} \times \nabla \Psi_t \right) = \mathbf{k} \cdot \nabla \times \bar{\mathbf{M}}_h. \tag{16}$$

Hence

$$\nabla \cdot \left(-\frac{1}{\mathscr{H}} \nabla \Psi_t \right) = G_z, \tag{17}$$

where $-G_z = \mathbf{k} \cdot \nabla \times \bar{\mathbf{M}}_h$ is the barotropic vorticity tendency. For simplicity we also call G_z the barotropic vorticity tendency.

Finally the horizontal current is computed by

$$\partial_t \mathbf{U}_h = \partial_t \bar{\mathbf{U}}_h + \partial_t \hat{\mathbf{U}}_h = \frac{1}{\mathscr{H}} \mathbf{k} \times \nabla \Psi_t + \partial_t \hat{\mathbf{U}}_h. \tag{18}$$

At each time step, equation (13) is solved explicitly to get the baroclinic part of the current. The elliptic equation (17) is solved to find Ψ_t, the barotropic part of the current.

There is no flux of momentum and heat across continental boundaries and at the bottom of the ocean; in addition, a no-slip boundary condition is currently used on the velocity field. The Poisson-like equation (17) is solved with Dirichlet conditions along continental boundaries, which means that no flux of mass is allowed through coastal boundaries. At the surface the momentum flux, the heat flux and the salinity flux (evaporation) are prescribed.

2.2.2. Numerical schemes. All the equations of the model are discretized, using a C-grid following the nomenclature of Arakawa and Lamb,[16] by a second-order (in time and space) finite difference method. With this representation, all the fields are discretized on a staggered grid where u, v, T, S and p are defined at the same level (Figure 1) and w is defined at intermediate vertical levels. The model uses an explicit temporal scheme based on the leap-frog second-order scheme combined with a stabilizing correction for the odd and even time modes.[17] The second-order spatially discretized Poisson problem for the barotropic streamfunction tendency is solved at each time step by a diagonally preconditioned conjugate gradient method which is well-adapted to vector computers.[18] For a given value of ε_r (see Tables I and II) the number of gradient iterations is defined by a convergence criterion satisfied by the Euclidean norm of residuals at each iteration l : $\|r^l\|/\|r^0\| \leqslant \varepsilon_r$.

Assuming that the variables $(u, v, w, p_H, T, S, \rho$ are known at time steps t_{n-1} and t_n, the variables are calculated at time step t_{n+1} by following the algorithm below.

1. Compute $\mathbf{M}_h^n$, $\bar{\mathbf{M}}_h^n$ and $(\partial_t \hat{\mathbf{U}}_h)^n$ by (13) explicitly.
2. Compute $(G_z)^n$ and solve (17) to obtain $(\Psi_t)^n$ and therefore $(\partial_t \bar{\mathbf{U}}_h)^n$.

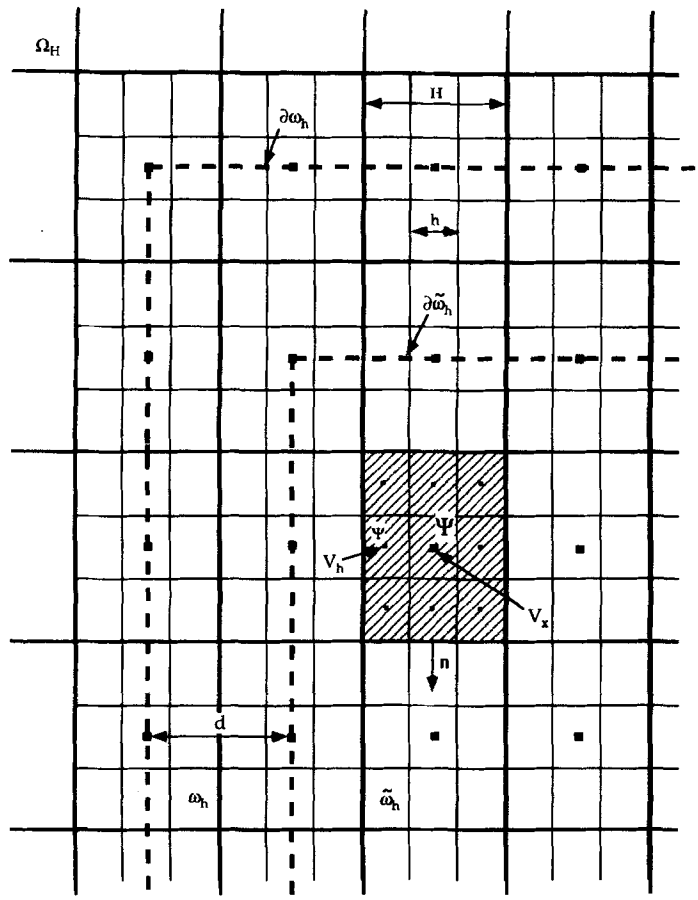

Figure 1(b). Non-matching nested grids Ω_H, ω_h and $\tilde{\omega}_h$. View of a corner of the local fine grid ω_h embedded inside the global coarse grid Ω_H. The correction subdomain $\tilde{\omega}_h \subset \omega_h$ is also represented in the case of $d = \text{dist}(\partial\tilde{\omega}_h, \partial\omega_h) = H$

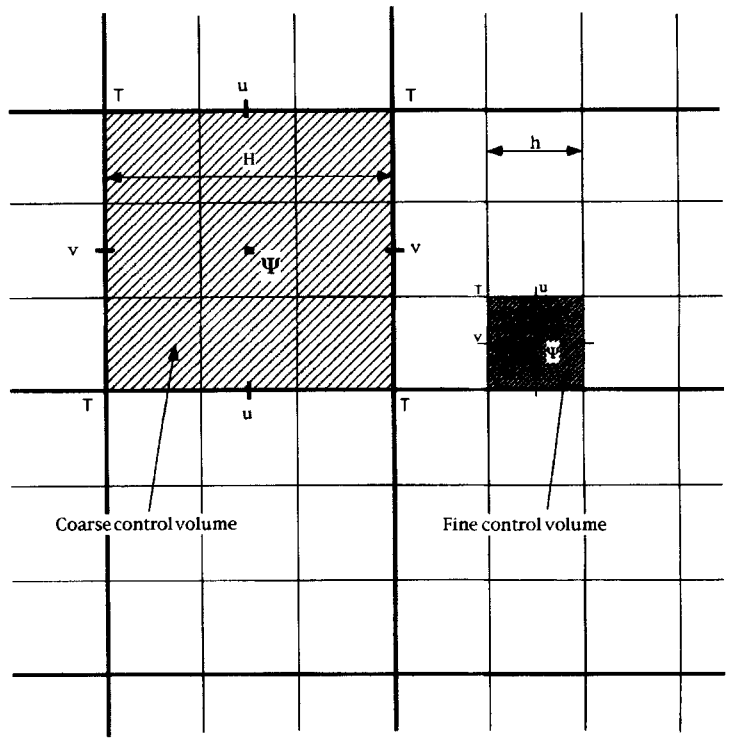

Figure 1(a). Staggered meshes in the horizontal plane (M, N). View of a part of Ω_H and ω_h, a coarse control volume with mesh step H and a fine control volume with mesh step h respectively, represented for a ratio $q = H/h = 3$; u and v are the horizontal velocity components, Ψ is the barotropic streamfunction located at the centre of the control volume, while the temperature nodes T are located at the vertices

3. Compute $(\partial_t \mathbf{U}_h)^n$ and integrate (18) explicitly to obtain $\mathbf{U}_h^{n+1} = (u^{n+1}, v^{n+1}, 0)$.
4. Solve (2) explicitly to obtain T^{n+1}.
5. Compute w^{n+1} with (8), ρ^{n+1} with the equation of state (5) and p_H^{n+1} with (9).

3. LOCAL GRID CORRECTION METHODS WITH MESH REFINEMENT

3.1. General methodology

The purpose of this paper is to compare three local resolution methods for the external mode, which represents the implicit part of the problem. The explicit part, i.e. the internal baroclinic mode, is calculated independently on the two grids and interpolations on the prognostic variables are made to calculate the global baroclinic tendency. The basic embedded model[1,2] uses two three-dimensional nested grids. Because of the two-dimensional nature of the streamfunction equation, we consider the global horizontal domain Ω with $\Gamma = \partial\Omega$ and a local refined domain ω, the zoom subdomain enclosed in Ω. The associated open discrete domains Ω_H and ω_h have respectively a coarse grid step H and a fine grid step h ($h < H$). We have chosen to use only odd grid ratios $q = H/h$ in order to simplify the interaction procedures between the grids (Figure 1(a)). With an odd grid ratio we have $\omega_H \subset \omega_h$ ($\omega_H = \omega \cap \Omega_H$), so that each temperature and velocity coarse grid point in the zoom domain coincides with a fine grid point of similar type. In particular, each coarse streamfunction

point Ψ in ω_H coincides with a fine streamfunction point in ω_h. Such a discretization induces a non-uniform composite grid on Ω (Figure 1(b)).

We introduce between the global coarse grid and the local fine grid a prolongation operator P_H^h and we define the discrete problems associated with equation (17), respectively global (P_Ω) and local (P_ω):

$$(P_\Omega) \quad \begin{cases} \nabla \cdot \left(-\dfrac{1}{\mathscr{H}} \nabla (\partial_t \Psi)_H \right) = (G_z)_H & \text{in } \Omega_H, \\ (\partial_t \Psi)_H = 0 & \text{on } \Gamma_H = \partial \Omega_H, \end{cases}$$

$$(P_\omega) \quad \begin{cases} \nabla \cdot \left(-\dfrac{1}{\mathscr{H}} \nabla (\partial_t \Psi)_h \right) = (G_z)_h & \text{in } \omega_h, \\ (\partial_t \Psi)_h = 0 & \text{on } \bar{\Gamma}_h = \partial \omega_h \cap \Gamma, \\ (\partial_t \Psi)_h = P_H^h [(\partial_t \Psi)_H] & \text{on } \Gamma_h = \partial \omega_h \backslash \bar{\Gamma}_h. \end{cases}$$

The 'forcing' procedure consists of prescribing the boundary conditions for the local grid ω_h from a previous global resolution on Ω_H. It is performed by interpolation of the coarse grid solution. In practice the prolongation P_H^h will be defined as a linear interpolation of type Q_1, reduced to a monodimensional operator on the interface Γ_h because the coarse and fine nodes are aligned (Figure 1(b)).

We also define a correction subdomain $\tilde{\omega} \subset \omega$ and the distance between their boundaries, $d = \text{dist}(\partial \tilde{\omega}, \partial \omega) \geqslant 0$, given by the number of coarse mesh steps, H (Figure 1(b)).

At each time step t_n, equation (17) is solved on the global and local grids. The general embedding procedure can be resumed by the following instructions.

1. Start:
   - $(G_z)_H^0 = (G_z)_H^n$ and $(G_z)_h^0 = (G_z)_h^n$ computed independently on Ω_H and ω_h
   - solve (P_Ω) with $(G_z)_H = (G_z)_H^0$ to give $(\partial_t \Psi)_H^0$
   - solve (P_ω) with $(G_z)_h = (G_z)_h^0$ to give $(\partial_t \Psi)_h^0$.
2. Two-grid iterations, $k = 1$ to K:
   - correction on the global grid by solving (P_Ω) with $(G_z)_H = (G_z)_H^k$ to give $(\partial_t \Psi)_H^k$
   - solve (P_ω) on the zoom grid with $(G_z)_h = (G_z)_h^k = (G_z)_h^0$ and new boundary conditions to give $(\partial_t \Psi)_h^k$.
3. Reactualization:
   - $(\partial_t \Psi)_H^n = (\partial_t \Psi)_H^K$ and $(\partial_t \Psi)_h^n = (\partial_t \Psi)_h^K$.

The general form of $(G_z)_H^k$ for the three local grid correction methods can be written for each coarse grid point $x \in \Omega_H$ as

$$(G_z)_H^k = (G_z)_H^0 + \chi_{\tilde{\omega}_H} d_H^k, \quad k \geqslant 1, \tag{19}$$

where $\chi_{\tilde{\omega}_H}$ is the characteristic function of $\tilde{\omega}_H$ and d_H^k is the local defect at iteration k.

Let us note that according to the previous algorithm, problems (P_Ω) and (P_ω) are both solved $K + 1$ times. The linearization phase is done implicitly at each time step because the terms G_z are not recomputed from the baroclinic deviations during the correction phase.

3.2. *Three local grid correction algorithms*

3.2.1. FIC Algorithm. The first multilevel local mesh refinement method is an adapted version of the so-called FIC (flux interface correction)[10,11] which was applied to the resolution of a barotropic modon.[14,15]

For each coarse node x of Ω_H in $\tilde{\omega}$ (i.e. $\forall x \in \tilde{\omega}_H$), $V_x = V_H(x)$ corresponds to the coarse control volume (with step H) and $\mathbf{n}$ is the external unit normal defined on its boundary ∂V_x (Figure 1(b)).

The principle of this algorithm is to satisfy, over a given control volume, a weak continuity relation of the solution fluxes between two non-matching grids of a composite mesh. In the adapted version[14] of the FIC algorithm we defined the correction by the local defect

$$d_H^k = r_H^k(\boldsymbol{\phi}) + (G_z)_H^{k-1} - (G_z)_H^0, \quad k \geqslant 1, \tag{20}$$

or more simply by

$$(G_z)_H^k = (G_z)_H^{k-1} + \chi_{\tilde{\omega}_H} r_H^k(\boldsymbol{\phi}), \quad k \geqslant 1, \tag{21}$$

where $\boldsymbol{\phi} = -(1/\mathscr{H})\nabla(\Psi_t)$ denotes the flux density vector of the barotropic streamfunction tendency and the residual is calculated by

$$r_H^k(\boldsymbol{\phi})(x) = \frac{\theta_{h,H}(x)}{\varepsilon_H(x)} \left(\frac{1}{\mathrm{mes}(\partial V_x)} \int_{\partial V_x} \boldsymbol{\phi}_h^{k-1} \cdot \mathbf{n} \mathrm{d}\sigma - \frac{1}{\mathrm{mes}(\partial V_x)} \int_{\partial V_x} \boldsymbol{\phi}_H^{k-1} \cdot \mathbf{n} \mathrm{d}\sigma \right). \tag{22}$$

We introduced the following quantities:

$$\theta_{h,H}(x) = 1 + \frac{\displaystyle\int_{V_x} (G_z)_H^k \mathrm{d}\mu - \int_{V_x} (G_z)_h^k \mathrm{d}\mu}{\displaystyle\int_{\partial V_x} \boldsymbol{\phi}_h^{k-1} \cdot \mathbf{n} \mathrm{d}\sigma - \int_{\partial V_x} \boldsymbol{\phi}_H^{k-1} \cdot \mathbf{n} \mathrm{d}\sigma}, \qquad \varepsilon_H(x) = \frac{\mathrm{mes}(V_x)}{\mathrm{mes}(\partial V_x)}. \tag{23}$$

This determination of $r_H^k(\boldsymbol{\phi})$, which corresponds to a conservative correction in terms of the solution flux, assumes that we take the following precaution:

$$\int_{\partial V_x} \boldsymbol{\phi}_h^{k-1} \cdot \mathbf{n} \mathrm{d}\sigma - \int_{\partial V_x} \boldsymbol{\phi}_H^{k-1} \cdot \mathbf{n} \mathrm{d}\sigma = 0, \quad \text{then } \mathrm{r_H^k}(\boldsymbol{\phi})(\mathrm{x}) = \frac{1}{\mathrm{mes}(\mathrm{V_x})} \left(\int_{\mathrm{V_x}} (\mathrm{G_z})_\mathrm{H}^\mathrm{k} \mathrm{d}\mu - \int_{\mathrm{V_x}} (\mathrm{G_z})_\mathrm{h}^\mathrm{k} \mathrm{d}\mu \right). \tag{24}$$

To compute the defect r_H^k, we use a linear restriction operator between the local grid and the global grid, of type FWICV (full weighting interface control volume), defined by

$$R_h^H(\boldsymbol{\phi}_h)(x) = \frac{1}{\mathrm{mes}(\partial V_x)} \int_{\partial V_x} \boldsymbol{\phi}_h \cdot \mathbf{n} \mathrm{d}\sigma, \quad \forall x \in \tilde{\omega}_H. \tag{25}$$

This operator is computed by a second-order quadrature formula corresponding to a spatial averaging of the fine flux at the interface ∂V_x:

$$R_h^H(\boldsymbol{\phi}_h)(x) \approx \frac{1}{\sum_{V_h \subset V_x} \mathrm{mes}(\partial V_h \cap \partial V_x)} \sum_{V_h \subset V_x} \boldsymbol{\phi}_h \cdot \mathbf{n} \mathrm{mes}(\partial V_h \cap \partial V_x). \tag{26}$$

For example, in the case of uniform square meshes it yields

$$R_h^H(\boldsymbol{\phi}_h)(x) \approx \frac{1}{4q} \sum_{V_h \subset qV_x} \boldsymbol{\phi}_h \cdot \mathbf{n}, \qquad \varepsilon_H = \frac{H}{4}. \tag{27}$$

In practice the quantity $\theta_{h,H}$ can be evaluated by successive approximations of (23) or, as in this study, by taking a constant relaxation coefficient[10] ($\theta_{h,H}(x) \approx \theta$, as $\forall x \in \tilde{\omega}_H$); here we chose empirically $\theta = 1$,[14] but the influence of θ was also investigated.[15]

The correction equation (21) can be applied in particular in the case of a non-exact resolution of problems (P_Ω) and (P_ω) by carrying out only a few iterations of the conjugate gradient solver but increasing the number K of correction iterations.

However, by using the Stokes theorem and considering that the Poisson problems are quasi-exactly solved (i.e. $\nabla \cdot \boldsymbol{\phi}_H^{k-1} \approx (G_z)_H^{k-1}, \forall k \geqslant 1$), we can show easily using (25) that the correction can be written as[15]

$$(G_z)_H^k = (1 - \chi_{\tilde{\omega}_H}\theta_{h,H})(G_z)_H^{k-1} + \chi_{\tilde{\omega}_H}\frac{\theta_{h,H}}{\varepsilon_H}R_h^H(\boldsymbol{\phi}_h^{k-1}), \quad k \geqslant 1. \tag{28}$$

More complete explanations of, some comments on and possible future extensions of the nested multilevel zoom FIC method are described in Reference 15.

3.2.2. LDC Algorithm. The second local grid correction method that will be tested is the LDC (local defect correction).[12,13] The correction is then defined by

$$d_H^k = L_H(\mathscr{R}_h^H((\partial_t\Psi)_h^{k-1})) - (G_z)_H^0, \tag{29}$$

where L_H is the discrete operator corresponding to the second-order elliptic operator $L = \nabla \cdot [-(1/\mathscr{H})\nabla]$ (L_H is calculated by a five-point finite different scheme as in the discrete problem corresponding to (P_Ω) and (P_ω)). The operator $\mathscr{R}_h^H$ is the FWCV[13] restriction defined by

$$\mathscr{R}_h^H(\vartheta_h)(x) = \frac{1}{\text{mes}(V_x)}\int_{V_x}\vartheta_h d\sigma, \quad \forall x \in \tilde{\omega}_H, \tag{30}$$

where ϑ_h represents any local variable. This operator is computed by a second-order quadrature corresponding to a spatial average of the fine grid quantities:

$$\mathscr{R}_h^H(\vartheta_h)(x) \approx \frac{1}{\sum_{V_h \subset V_x}\text{mes}(V_h)}\sum_{V_h \subset V_x}\vartheta_h\text{mes}(V_h), \quad \forall x \in \tilde{\omega}_H. \tag{31}$$

In the case of uniform square meshes it gives

$$\mathscr{R}_h^H(\vartheta_h)(x) \approx \frac{1}{q^2}\sum_{V_h \subset V_x}\vartheta_h, \quad \forall x \in \tilde{\omega}_H. \tag{32}$$

3.2.3. DM Algorithm. The third local grid correction method that will be tested is the technique used by some authors for oceanography[6,7] nested models, whereas improved versions of the 'box' method have been generally used in meteorology.[3,4] We shall use the initials DM to refer to this direct method. The correction is then defined by[6]

$$d_H^k = \mathscr{R}_h^H((G_z)_h^0) - (G_z)_H^0. \tag{33}$$

Let us remark that in any case the correction does not depend on the index k. Therefore the main difference with respect to two previous methods is that the DM algorithm is a direct method. Thus we are better to write the correction by the equality

$$(G_z)_H^C = (G_z)_H^n + \chi_{\tilde{\omega}}[\mathscr{R}_h^H((G_z)_h^n) - (G_z)_H^n]. \tag{34}$$

In fact, at any time step t_n, equation (17) is solved on the two grids in the following way.

(a) Solve (P_Ω) with $(G_z)_H = (G_z)_H^C$ to give $(\partial_t \Psi)_H^n$.
(b) Solve (P_ω) with $(G_z)_h = (G_z)_h^n$ to give $(\partial_t \Psi)_h^n$.

Therefore the correction just consists of a simple reactualization of the coarse barotropic vorticity tendency by means of a local average of the barotropic vorticity tendency on the fine grid.

3.3. *Differences and common features*

The multigrid extension can be easily achieved by a recursive implementation of the two-grid algorithm in the form of V- or W-cycles.[13]

In contrast with both the LDC and FIC iterative methods, the DM method is direct. With the LDC and FIC we can solve the elliptic problems (P_Ω) and (P_ω) by means of an 'inexact solve' procedure. On the other hand, the correction can be applied directly once and once only, without any initialization phase, with the DM. This is possible because the barotropic vorticity tendency (G_z) can be computed independently on the two grids before solving problems (P_Ω) and (P_ω).

To evaluate $R_h^H(\phi_h)$ for the FIC algorithm in the case of non-constant $\mathscr{H}$, it would be better to use equality (26) together with a conservative discretization method.[10] However, if the depth is constant, as in the two tests of Section 4, and if the local problems are quasi-exactly solved (i.e. $\nabla \cdot \boldsymbol{\phi}_h^k \approx (G_z)_h^k, \forall k \geqslant 0$), we can compute this term by a volume average on V_x (restriction of type FWCV) instead of a surface average on ∂V_x, so[15]

$$\frac{1}{\varepsilon_H(x)} R_h^H(\boldsymbol{\phi}_h^k)(x) \approx \frac{1}{\sum_{V_h \subset V_x} \mathrm{mes}(V_h)} \sum_{V_h \subset V_x} (G_z)_h^k \mathrm{mes}(V_h). \tag{35}$$

In that case and for the parameters $\theta_{h,H} = 1$ and $K = 1$, if we use the more general equation (28), we find the correction term applied on the global grid with the DM (34) as

$$(G_z)_H^1 \approx (1 - \chi_{\tilde{\omega}_H})(G_z)_H^0 + \chi_{\tilde{\omega}_H} \frac{1}{\sum_{V_h \subset V_x} \mathrm{mes}(V_h)} \sum_{V_h \subset V_x} (G_z)_h^0 \mathrm{mes}(V_h). \tag{36}$$

Finally, let us remark that with the FIC method, if the correction terms are evaluated on the coarse nodes of the local boundary, i.e. $\partial\omega_H$, the algorithm allows us to ensure the conservation of fluxes between the two domains.[10] This property will be important to ensure, upon long-time integration in basin-scale climate studies, the conservation of energy and heat or momentum fluxes at the interface between the nested subdomains. For the present study where the FIC method is only applied to the barotropic part of the horizontal velocity, the conservation of the barotropic energy and momentum flux is ensured at the scale of each coarse control volume located in the correction subdomain $\tilde{\omega}$.

4. NUMERICAL RESULTS

The three local grid correction algorithms with mesh refinement are applied to two non-stationary problems proposed by Spall and Holland:[6] a barotropic modon and an anticyclonic baroclinic vortex. They were motivated by the knowledge of their expected behaviour and their highly non-linear and pathological eddy. The results will be very sensitive to errors and therefore they provide strong tests of the local grid correction methods. In the first case the modon is initialized at the centre of the local domain by giving the analytical solution of the barotropic streamfunction.[19] It propagates towards the east into the global domain through the zoom grid boundary under the beta planetary effect. This test supplies a good benchmark for the problem of open boundary conditions. Initially, all the flow field is contained within the fine grid. The coarse grid must give good boundary conditions to the zoom grid to maintain the structure of the modon when it goes through the grid interface. Moreover, the

boundary condition obtained from the global grid will depend on the sharp resolution of the local problem and the effective correction for the coarse grid. The second test problem deals with the propagation of an anticyclonic baroclinic vortex. It also starts with information within the local domain and then it generates large-scale features which may come back by reflection according to the boundary conditions on the global domain. It provides new forcing conditions for the evolution of the local solution. Besides, this problem allows us to investigate the baroclinic aspects for the local grid correction with a stratified ocean where important internal gravity waves are also present.

4.1. Notation

For any characteristic variable φ of the problem, i.e. the barotropic streamfunction Ψ, the kinetic energy E_c and the density ρ or temperature T, φ^* represents the reference solution, which is either the analytic solution (in the case of the barotropic modon) or the numerical solution calculated with a high resolution (for the baroclinic vortex). We evaluate as a function of time $t_n = n\Delta t$ the discrete error on the global grid at the zoom iteration k, defined by $e_H^{k,n} = \varphi_H^{*,n} - \varphi_H^{k,n}$. By choosing the L^2 discrete norm, we consider as a function of time and for the mesh ratio $q = 3$ the quantities $\xi_H^{k,n} = \|e_H^{k,n}\|/\|\varphi_H^{*,n}\|$, which represent the relative error discrete norms. We also compute the errors on the local grid, $\xi_h^{k,n} = \|e_h^{k,n}\|/\|\varphi_h^{*,n}\|$, in a similar way.

When the index k is omitted, it means that the errors are computed without zoom, i.e. the monodomain global resolution with a large grid step H or even with the fine grid step h (without correction). When $k = 0$, it means that the errors are calculated on the local solution obtained without correction for the global coarse grid, i.e. with the passive version of the nested model. Note that we always have $k = 1$ for the DM.

Finally, for the two iterative methods (FIC and LDC) we define an asymptotic rate of convergence at each time step by

$$\rho_n^K = \left(\frac{\|\delta_H^{K,n}(\Psi_t)\|}{\|\delta_H^{1,n}(\Psi_t)\|} \right)^{1/(K-1)},$$

where $\delta_H^{k,n}(\Psi_t) = (\Psi_t)_H^k - (\Psi_t)_H^{k-1}$, $(\Psi_t)_H^k$ being the value obtained at time $n\Delta t$ for the kth iteration of the local grid correction algorithm LDC or FIC. A more standard definition of the covergence rate for an iterative procedure has also been used in References 14 and 15, but only for the FIC method for which the flux residual tends to zero, which is not the case for the LDC:

$$\tilde{\rho}_n^K = \left(\frac{\|r_H^{K,n}(\boldsymbol{\phi})\|}{\|r_H^{1,n}(\boldsymbol{\phi})\|} \right)^{1/(K-1)}.$$

The convergence rate is estimated by an 'inexact solve', i.e. for a small fixed number of conjugate gradient iterations for the resolution of (P_Ω) on the CG ($Npcg_H$) and for the resolution of (P_ω) on the FG ($Npcg_h$), if K is sufficiently large; typically $K = 10$ V-cycles.

4.2. A barotropic modon

The barotropic modon is initialized at time $t = 0$ on both grids by the analytical solution of the quasi-geostrophic potential vorticity equation with the beta plane approximation in an infinite ocean.[19] At weak Rossby numbers this solution can be taken as a reference to compute the errors of simulations on a large global domain and with sufficiently small diffusion parameters. The global resolution domain is considered as a homogeneous ocean. The modon is initially centred in the local domain ω, which is itself centred within the global domain (Figure 2). With the beta planetary effect

at the middle latitude $\theta_m = 38 \cdot 5°$ N, the modon of radius $a = 75$ km propagates eastwards without any deformation at the uniform speed $C = \beta a^2 \approx 0 \cdot 1$ m s^{-1}, where β is given by

$$\beta = \frac{2\Omega}{a_r} \cos(\theta_m),$$

with Ω the rotation of the Earth and a_r the radius of the Earth.

The global discrete domain Ω_H covers 750 km by 750 km with a constant grid step $H = 15$ km for the CG and the local domain is 300 km by 300 km with a step $h = 5$ km for the FG, the ratio being $q = 3$. With respect to the CFL stability criterion the simulations are performed with $\Delta t = 7200$ s and carried out over 350 time steps, i.e. 29 days 4 h.

In Figure 3 we have represented, at different times, lines of iso-Ψ on ω_h. We have chosen to show only, in the zoom case, the result produced by the FIC algorithm for $\theta = 1$ and $K = 1$. The other algorithms produce globally the same behaviour as the local zoom solution. The modon crosses quite well the boundary $\partial\omega$ between the two domains with a very weak diffusion and deformation. It also leaves the fine grid region with a weak trace of its crossing and with a small delay compared with the analytical propagation speed, which is approximately 3% faster than the nested grid model solution evaluated on the fine grid. For the global solution the analytical speed of propagation is approximately 10% faster than the one obtained on the coarse grid with zoom correction. For the monodomain solution on the coarse grid without zoom this difference is of the order of 23%. These results are in agreement with the study of McWilliams *et al.*,[20] which shows that there is little practical utility in increasing the number of grid nodes per modon diameter beyond 30. For that reason and because we have already carried out this simulation with a finer nested subgrid,[14,15] we have chosen only one value for q in the present work.

The noticeable improvement in the precision with zoom can be verified with the relative errors computed on Ω_H (Figure 4). A comparison of the results obtained with the three methods is shown in

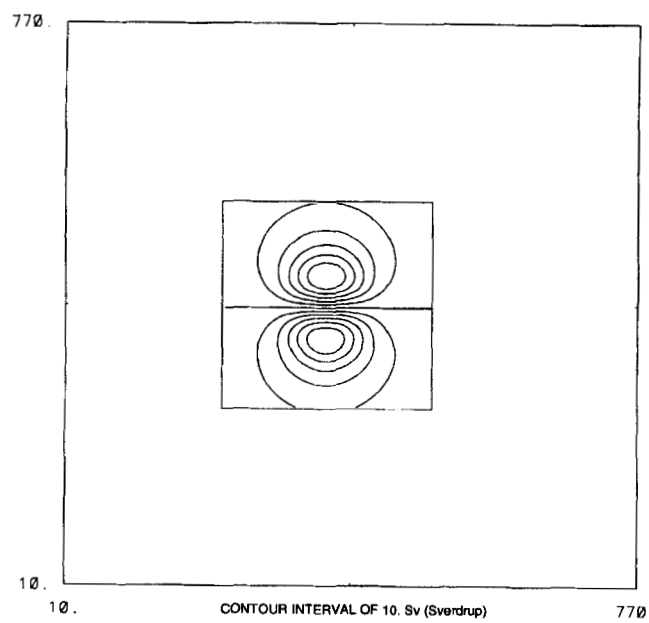

Figure 2. Initial position of the modon; lines of iso-Ψ on ω_h. The global Ω and local ω domains are represented

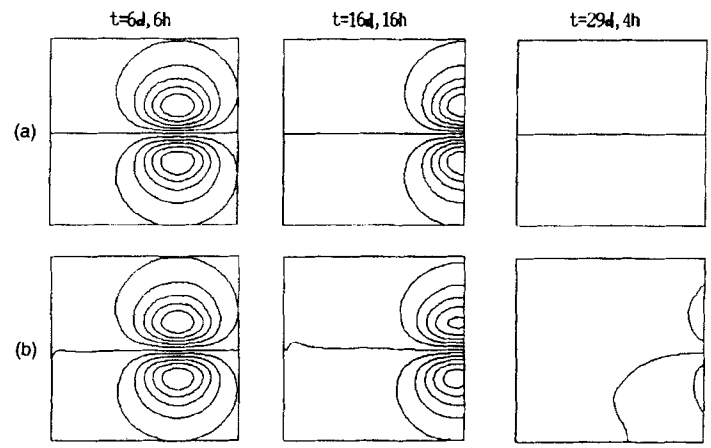

Figure 3. Barotropic modon; lines of iso-Ψ on ω_h at time 6 days 6 h, 16 days 16 h and 29 days 4 h. (a) Analytical solution. (b) FIC with $d = H$ and $K = 1$

Figures 5 and 6, where the errors are evaluated with the optimal parameter $d = H$ for the DM, LDC and FIC and with one iteration of the zoom algorithm at each time step. The behaviour of the solution on Ω_H and on ω_h obtained with the FIC and DM is very similar, according to the remark in Section 3.3; the error found with the LDC is a little greater. Note that the error with zoom effect on ω_h, whatever the method used (Figure 6), is of the order of the one obtained with a more expensive

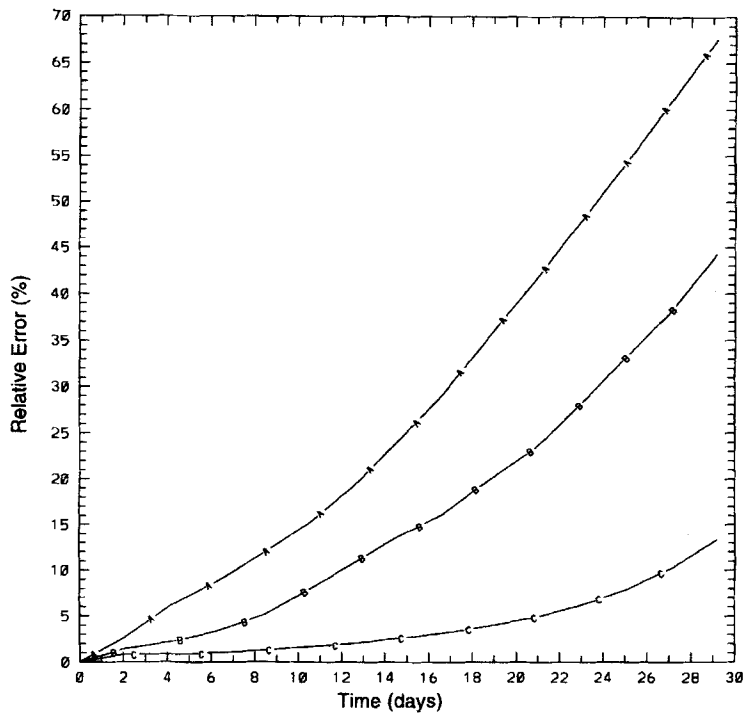

Figure 4. Barotropic modon; relative error for Ψ on Ω_H. A. Monodomain on Ω_H: ξ_H^n. B. FIC, $K = 1, d = H$: $\xi_H^{1,n}$. C. Monodomain on Ω_h: ξ_h^n

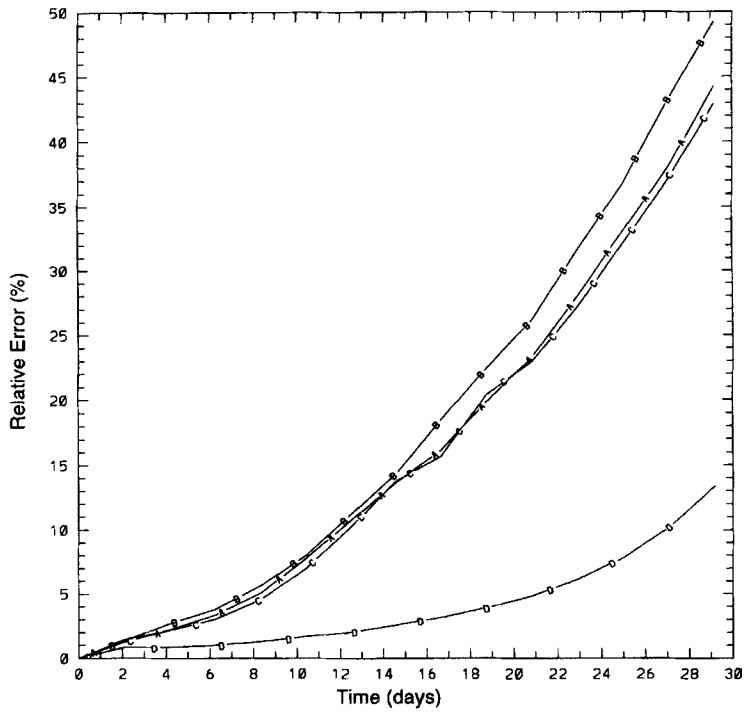

Figure 5. Barotropic modon; relative error for Ψ on Ω_H. A. FIC, $K = 1, d = H$: $\xi_H^{1,n}$. B. LDC, $K = 1, d = H$: $\xi_H^{1,n}$. C. DM, $d = H$: $\xi_H^{1,n}$. D. Monodomain on Ω_h: ξ_h^n

computation on the single global grid Ω_h (Figure 5). The cost in CPU time of the use of a high resolution (Ω_h) over the entire domain is 1·6 times greater than for the embedded model with the LDC or FIC method and 2·6 times larger than with the DM (see Table I). Increasing the iteration number K of the zoom algorithm does not improve significantly the resulting solution given by the LDC or FIC, as we can see in Figures 7 and 8, as long as a quasi-exact solve is performed for the resolution of both the global and local problems.

In order to evaluate the influence of the parameter d, we have computed the errors on Ω_H with $d = H, 2H$ and $5H$ for the DM, FIC and LDC (Figures 9–11 respectively). The results are relatively sensitive to the choice of d. The optimal value is $d = H$ for all three methods. We can verify again that the solutions found with the DM and FIC for the different values of d are very similar. The value $d = 5H$ gives poor results because of the small number of coarse grid nodes affected by the zoom correction. The most significant difference occurs for $d = 2H$: for the LDC this value gives a slightly greater error than the optimal value $d = H$; for the FIC and DM this choice induces a particular behaviour of the solution. On one hand, until the 15th day the error in the global solution with $d = 2H$ is almost equal to the one obtained with the optimal value $d = H$. On the other hand, between the 15th and 17th day, when the modon centre crosses the interface, the error with $d = 2H$ increases more and finally exceeds that found with $d = 5H$.

The computation of the convergence rate by the inexact solve, with $Npcg_H = 8$ and $Npcg_h = 12$ at each time step $t_n = n\Delta t$, gives the time variation in ρ_n^{10} for the LDC (Figure 12) and FIC (Figure 13(a)). The convergence rate of the FIC varies in the range 0·35–1 when the modon is fully outside the zoom subdomain. For the LDC until the 210th time iteration this rate is between 0·3 and 0·4. After this time step and until the end the rate is subject to variations between 0·4 and 0·9. However,

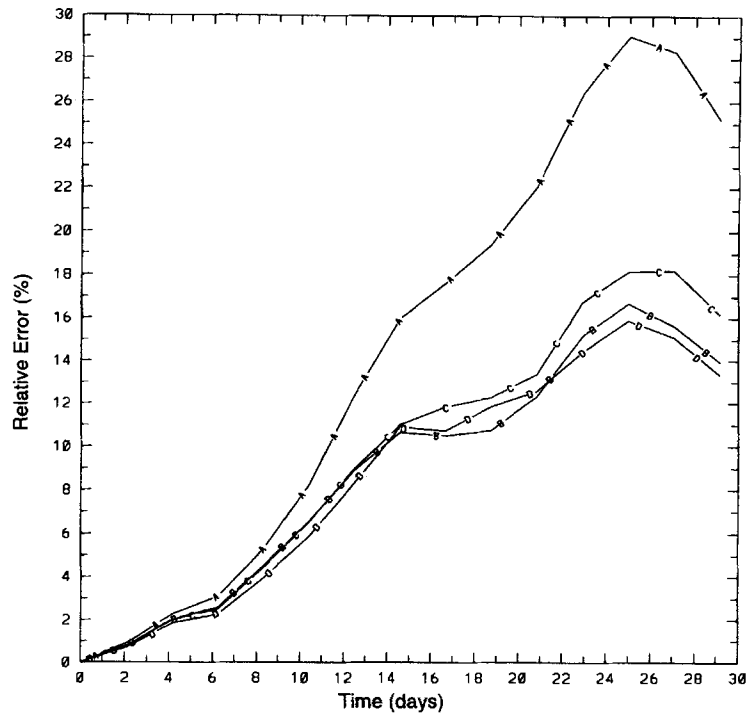

Figure 6. Barotropic modon; relative error for Ψ on ω_h. A. Passive nested grid model: $\xi_h^{0,n}$. B. FIC, $K=1, d=H$: $\xi_h^{1,n}$. C. LDC, $K=1$, $d=H$: $\xi_h^{1,n}$. D. DM, $d=H$: $\xi_h^{1,n}$

Table I. Parameters for nested grid model and CPU times for simulation of barotropic modon

Parameter	FG	CG	RG
$M, N(L=1)$	61	51	152
Δt (s)	7200	7200	7200
$\Delta x, \Delta y$ (km)	$h=5$	$H=15$	$h=5$
ε_r	10^{-2}	10^{-2}	10^{-2}
$\nu_{th}=\kappa_{th}$ (m^2 s^{-1})	25	40	25

Numerical model	CPU time (s) ($d=H$)	Iterations in time
Monodomain on Ω_H	6	350
Monodomain on Ω_h	36	350
DM	13·7	350
FIC, $K=1$	22·2	350
LDC, $K=1$	21·3	350
FIC, $K=2$	24	350
LDC, $K=2$	24	350
FIC, $K=10$ (inexact solve)	55·4	350
LDC, $K=10$ (inexact solve)	56·2	350

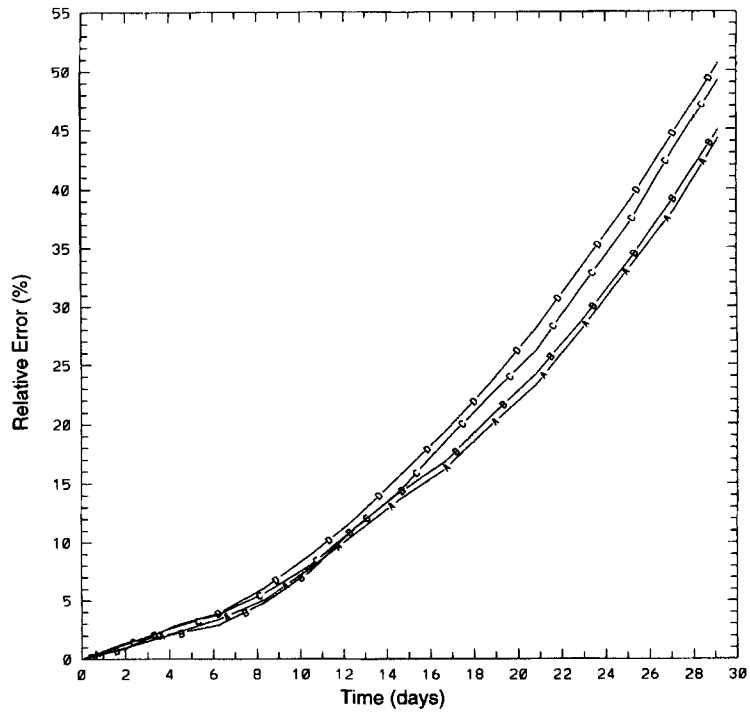

Figure 7. Barotropic modon; relative error for Ψ on Ω_H. A. FIC, $K = 2, d = H$: $\xi_H^{2,n}$. B. FIC, $K = 1, d = H$: $\xi_H^{1,n}$. C. LDC, $K = 2, d = H$: $\xi_H^{2,n}$. D. LDC, $K = 1, d = H$; $\xi_H^{1,n}$

we must notice that a far better result was obtained on the same modon problem for the FIC algorithm by using the more classical definition of the convergence rate $\tilde{\rho}$ in Section 4.1 involving the ratio of the successive residuals norms (Figure 13(b)). Thus for the FIC method the mean convergence rate is as good as 0·03 with variations between 0·01 and 0·06 up to the 300th time step and especially very small variations around 0·03 when the modon is still included inside the local zoom grid. After the 300th time step the convergence rate is increasing but not beyond the value 0·2 (see Figure 13(b)).

4.3. A baroclinic vortex

The nested grid model is initialized on both grids by a Gaussian pressure distribution with a horizontal e-folding scale of 50 km in the upper layer and no motion in the lower layer. The thermocline is located at a depth of 80 m and the elevation height of the pycnocline is 40 m. The velocity field is initialized to be in geostrophic balance with the Gaussian pressure distribution. This equality is verified in a discrete way in Ω_H and ω_h, so that at any level the velocity is a non-divergent field. Therefore the transport is non-divergent at time $t = 0$ on both grids. It is important to satisfy this property in order to conserve in the discrete model, at each time step, a non-divergent transport. In this study the solution includes a high non-geostrophic component, the Rossby number $R\sigma$ being initially equal to 0·3. Under the beta planetary influence the anticyclonic vortex located in the northern hemisphere ($\theta_m = 38 \cdot 5°$ N) moves to the southwest.

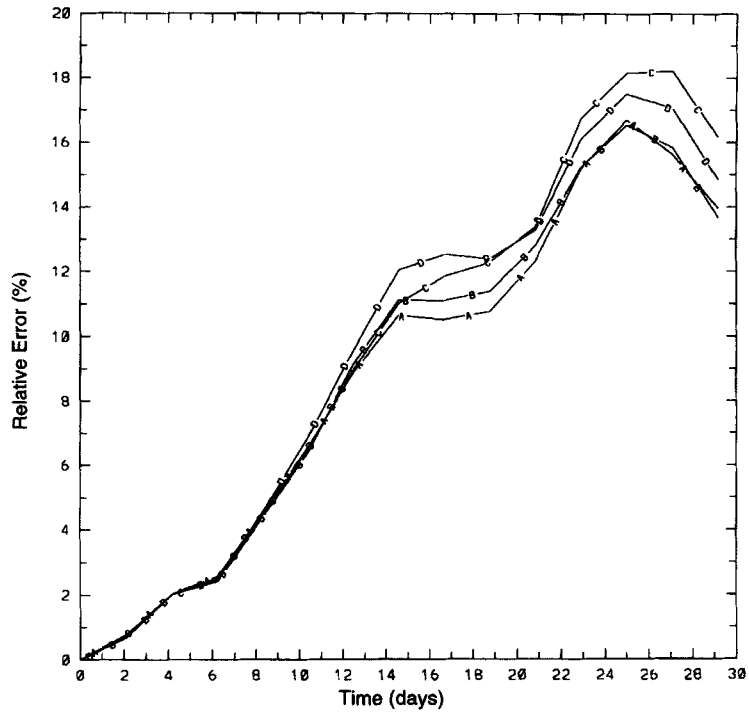

Figure 8. Barotropic modon; relative error for Ψ on ω_h. A. FIC, $K = 2, d = H$: $\xi_h^{2,n}$. B. FIC, $K = 1, d = H$: $\xi_h^{1,n}$. C. LDC, $K = 2, d = H$: $\xi_h^{2,n}$. D. LDC, $K = 1, d = H$: $\xi_h^{1,n}$

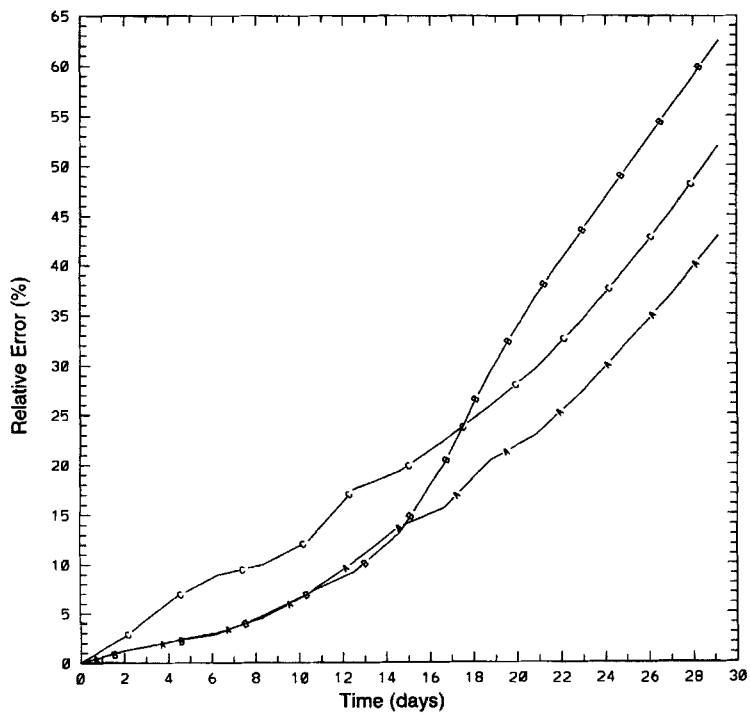

Figure 9. Barotropic modon; relative error for Ψ on Ω_H. A. DM, $d = H$: $\xi_H^{1,n}$. B. DM, $d = 2H$: $\xi_H^{1,n}$. C. DM, $d = 5H$: $\xi_H^{1,n}$

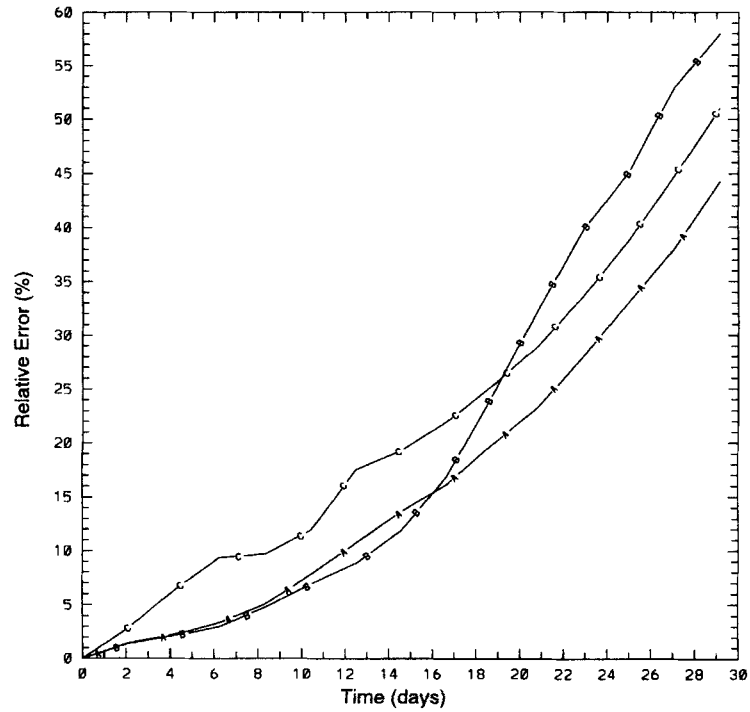

Figure 10. Barotropic modon; relative error for Ψ on Ω_H. A. FIC, $K = 1, d = H$: $\xi_H^{1,n}$. B. FIC, $K = 1, d = 2H$: $\xi_H^{1,n}$. C. FIC, $K = 1, d = 5H$: $\xi_H^{1,n}$

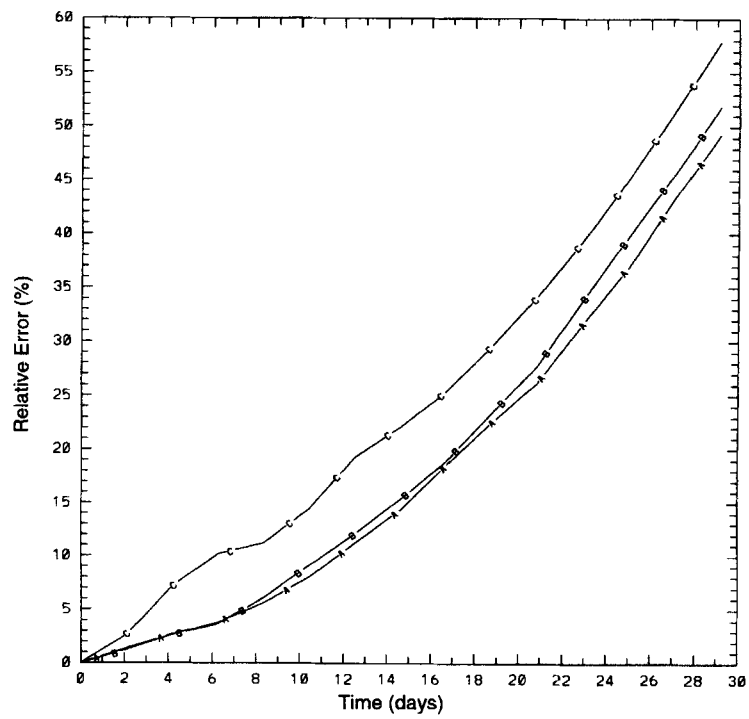

Figure 11. Barotropic modon; relative error for Ψ on Ω_H. A. LDC, $K = 1, d = H$: $\xi_H^{1,n}$. B. LDC, $K = 1, d = 2H$: $\xi_H^{1,n}$. C. LDC, $K = 1, d = 5H$: $\xi_H^{1,n}$

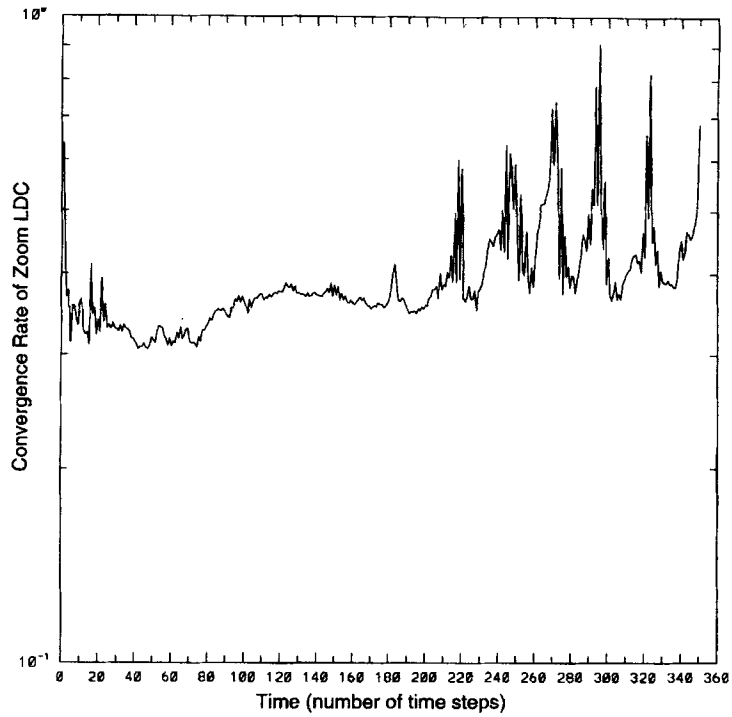

Figure 12. Barotropic modon; convergence rate for LDC: ρ_n^{10}

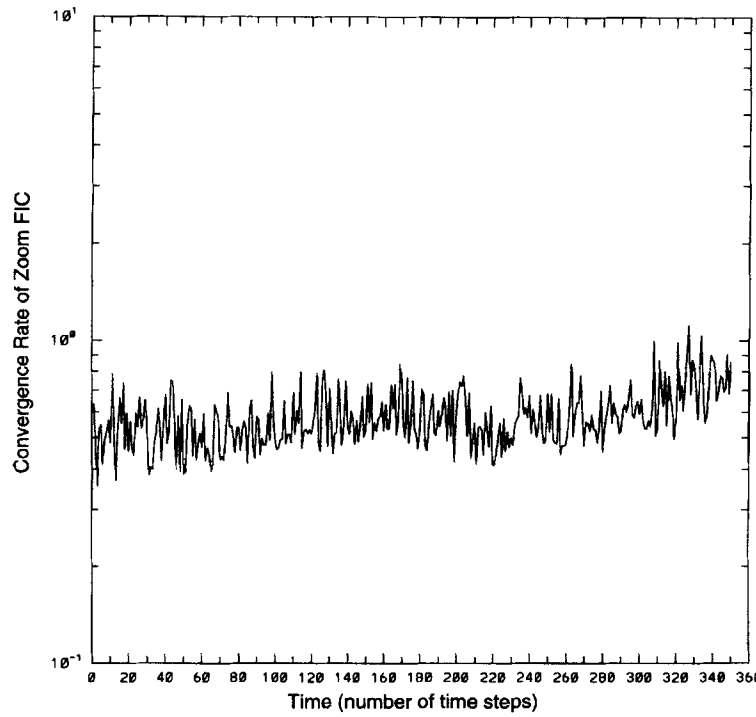

Figure 13(a). Barotropic modon; convergence rate for FIC: ρ_n^{10}

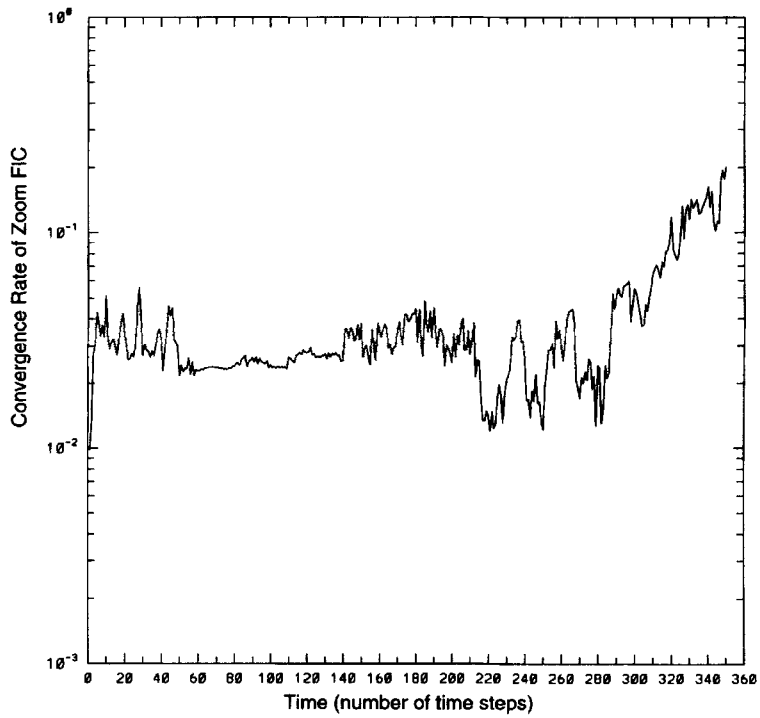

Figure 13(b). Barotropic modon; convergence rate for FIC: $\tilde{\rho}_n^{10}$

There is no analytic solution available for the evolution of such a baroclinic vortex. Hence the reference solution will be the numerical solution computed with the basic model with the single fine grid on Ω, corresponding to the discrete domain Ω_h, which we shall call the reference grid (RG).

Initially the vortex is centred inside a closed ocean without topography and with rectilinear lateral boundaries. The dimension of the global domain Ω is 675 km by 675 km horizontally and the depth is 550 m. The dimension of the local domain ω is 200 km by 200 km. The coarse grid (CG) is defined by a 45×45 mesh on the horizontal level ($M \times N$) with a constant grid step $H = 15$ km and by 10 resolution levels (L) in the vertical direction. Only the ratio $q = 3$ was used, inducing for the fine grid (FG) a horizontal grid step $h = 5$ km for a 40×40 mesh on the horizontal level. The simulations are performed with $\Delta t = 1200$ s, satisfying the CFL stability criterion, and carried out over 9000 time steps, i.e. 125 days.

We have represented in Figure 14 the density ($\delta\rho = \rho - 1000$) on ω_h at the pycnocline level, i.e. at a depth of 112 m, for the reference solution (Figure 14(a)) and the fine grid solution (Figure 14(b)) obtained by the nested model with the DM for the resolution of the barotropic part. Globally the vortex propagates towards the south-west with a relatively large vertical diffusion. The propagation speed of the baroclinic vortex decreases rapidly, correlatively with the maximum of vorticity which decreases from the value $2 \cdot 8 \times 10^{-5}$ s^{-1} at $t = 0$ to the value $0 \cdot 35 \times 10^{-5}$ s^{-1} at $t = 125$ days. The vortex develops some instability which creates a cyclonic circulation visible at the south-west and north-west of the vortex centre (Figure 15(a)). The barotropic part of the current is represented in Figure 16 for the coarse grid solution with zoom and without zoom correction. These solutions may be compared with the expensive solution obtained on the RG, which requires four times more CPU time than the nested grid solution (see Table II). The coarse grid solution with zoom looks very

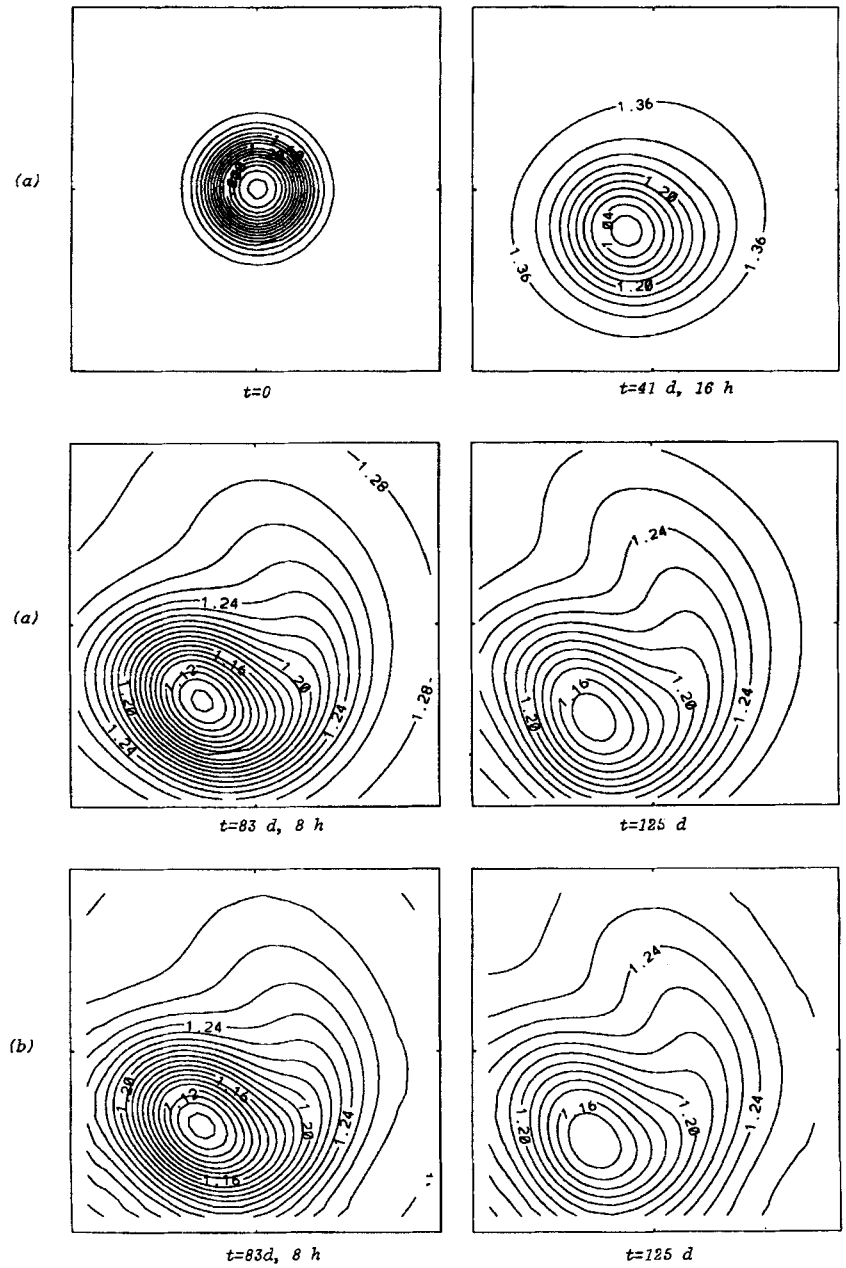

Figure 14. Reference and fine grid calculations; density of the baroclinic vortex at depth $z = -112$ m. (a) Reference calculation; $\delta\rho = \rho - 1000$ (g) contours on ω_h at time 0 (contour interval CINT $= 1 \times 10^{-1}$), 41 days 16 h (CINT $= 4 \times 10^{-2}$), 83 days 8 h (CINT $= 1 \times 10^{-2}$) and 125 days (CINT $= 1 \times 10^{-2}$). (b) Fine grid calculation with zoom correction; $\delta\rho = \rho - 1000$ (g) contours on ω_h (same CINT values as in (a)) at time 83 days 8 h and 125 days

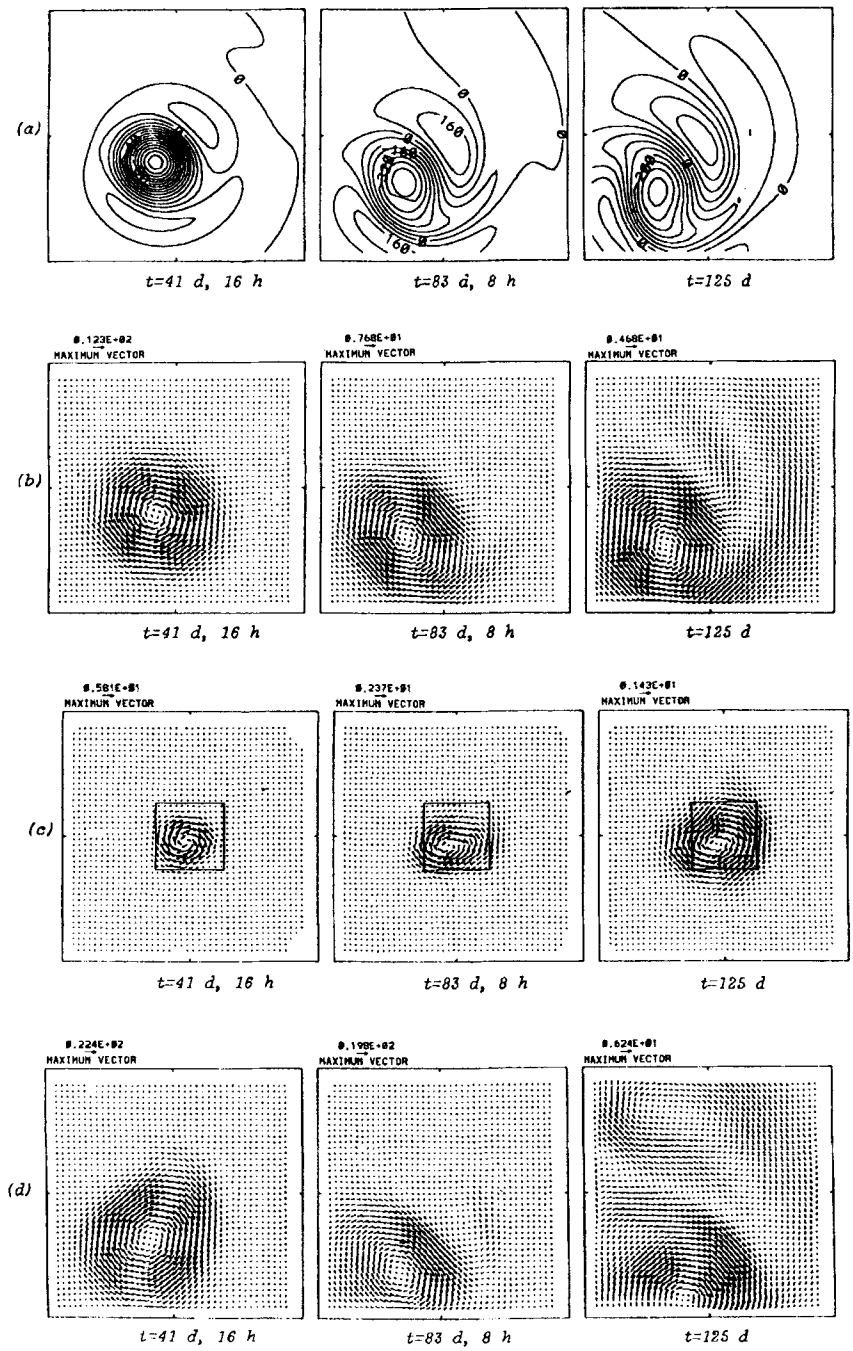

Figure 15. Reference, fine and coarse grid calculations for the baroclinic vortex at depth $z = -7$ m ($Ro = 0{\cdot}3$ for (a)–(c)). (a) Reference calculation; vorticity contours $\zeta = \partial_x v - \partial_y u$ (s^{-1}) on ω_h at time 41 days 16 h (CINT $= 1 \times 10^{-6}$, labels scaled by 10^7), 83days 8 h (CINT $= 8 \times 10^{-7}$, labels scaled by 10^8) and 125 days (CINT $= 5 \times 10^{-7}$, labels scaled by 10^8). (b) Fine grid calculation with zoom correction; horizontal velocity $\mathbf{U}_h$ (cm s^{-1}) on ω_h at time 41 days 16 h, 83 days 8 h and 125 days. (c) Coarse grid calculation without zoom; horizontal velocity $\mathbf{U}_h$ (cm s^{-1}) on Ω_H at time 41 days 16 h, 83 days 8 h and 125 days. The boundary of the local domain is indicated. (d) Fine grid calculation with zoom correction for the baroclinic vortex with $Ro = 0{\cdot}5$; horizontal velocity $\mathbf{U}_h$ (cm s^{-1}) on ω_h at time 41 days 16 h, 83 days 8 h and 125 days

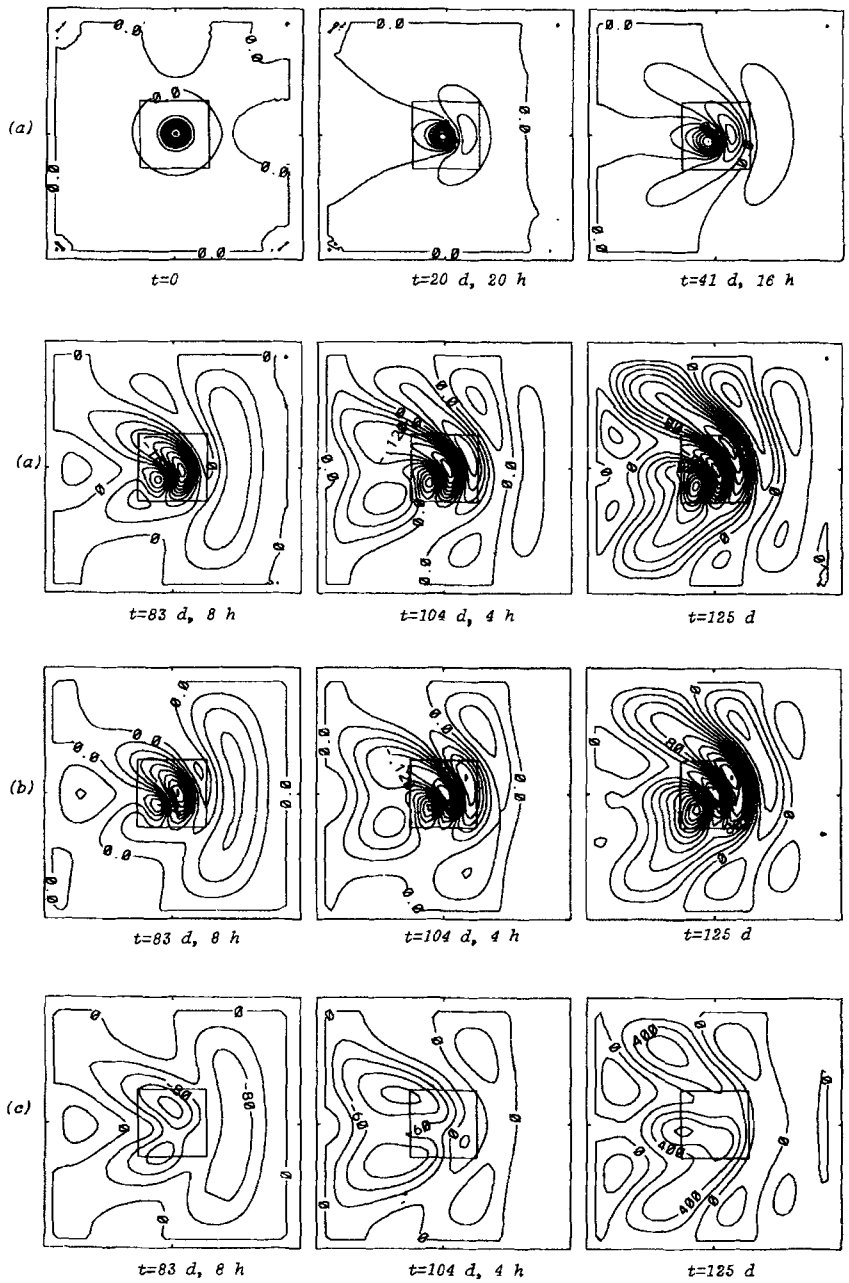

Figure 16. Reference and coarse grid calculations for the baroclinic vortex; the local domain is indicated. (a) Reference calculation; streamfunction contours (Sv) on Ω_h at time 0 (CINT $= 1 \times 10^{-1}$), 20 days 20 h (CINT $= 9 \times 10^{-2}$), 41 days 16 h (CINT $= 6 \times 10^{-2}$), 83 days 8 h (CINT $= 4 \times 10^{-2}$), 104 days 4 h (CINT $= 3 \times 10^{-2}$) and 125 days (CINT $= 2 \times 10^{-2}$, labels scaled by 10^3). (b) Coarse grid calculation with zoom; streamfunction contours (Sv) on Ω_H (same CINT values as in (a)) at time 83 days 8 h, 104 days 4 h and 125 days (labels scaled by 10^3). (c) Coarse grid calculation without zoom; streamfunction contours (Sv) on Ω_H (same CINT values as in (a)) at time 83 days 8 h, 104 days 4 h and 125 days (labels scaled by 10^4)

Table II. Parameters for nested grid model and CPU times for simulation of baroclinic vortex

Parameter	FG	CG	RG
M, N	40	45	134
L	10	10	10
Δt (s)	1200	1200	1200
$\Delta x, \Delta y$ (km)	$h = 5$	$H = 15$	$h = 5$
ϵ_r	10^{-2}	10^{-2}	10^{-2}
$v_{th} = \kappa_{th}$ (m^2 s^{-1})	50	125	50
$v_{tz} = \kappa_{tz}$ (m^2 s^{-1})	5×10^{-4}	5×10^{-4}	5×10^{-4}

Numerical model	CPU time (s) (d = 0)	Iterations in time
Monodomain on Ω_H	572	9000
Monodomain on Ω_h	4335	9000
DM	1148	9000
FIC, $K = 2$	1355	9000
LDC, $K = 2$	1355	9000

similar to the reference one, in contrast with the coarse monodomain solution without zoom. The solution rapidly develops barotropic Rossby waves which extend towards the open boundary of the local domain and involve the entire domain. Finally, at $t = 125$ days the solution is quite complicated and the initial structure of the barotropic ring is no longer recognizable.

The propagation across the interface between the two grids is reproduced quite well by the nested grid model without any distortion of the solution (Figure 16(b)). Without the zoom effect the solution diverges rapidly from the reference solution, as we can see in Figures 15(c) and 16(c), where the horizontal surface velocity and the barotropic streamfunction are represented respectively. In the case of the coarse monodomain resolution on Ω_H there are only six grid nodes across the vortex diameter. This resolution is widely non-sufficient to solve correctly the propagation of the vortex, as we can see in Figures 17(a) and 17(b), where the kinematic energy ($E_c(x, y, z) = u^2(x, y, z) + v^2(x, y, z)$) relative error is represented in the cases with zoom and without zoom correction on the coarse and the fine grid respectively. The zoom effect is quite spectacular: with feedback the relative error varies with time from only 5% to 23% on Ω_H and from 0% to 20% on ω_h; without zoom the error increases rapidly to reach the maximal value of 90% on the coarse grid and 62% on the fine grid. A similar spectacular reduction of the error is observed with zoom on the temperature or density on Ω_H (Figure 18(a)) and on ω_h (Figure 18(b)).

Let us notice that because of the correction made on the velocity field to ensure the non-divergent transport hypothesis in a discrete way on Ω_H, the initial value of the relative error on Ω_H (Figure 17(a)) is not zero (approximately 10%). Thus the initial discrete horizontal velocity field on Ω_H is not the exact identity restriction of this on Ω_h at time $t = 0$. We can see that the first effect of feedback ($t = 0$–40 days, Figure 17(a), curve B) is to constrain the global solution to tend to the reference solution.

With the zoom DM for different values of the parameter d and without zoom the relative errors for the kinetic energy on the CG are represented in Figures 19 and 20. Approximately until the 25th day the coarse grid solutions calculated with $d = 0$, H and $2H$ are similar and the errors are far lower than the one obtained with the coarse monodomain solution. After this time the error in the solution calculated with $d = H$ or $2H$ begins increasing rapidly and finally exceeds the monodomain solution

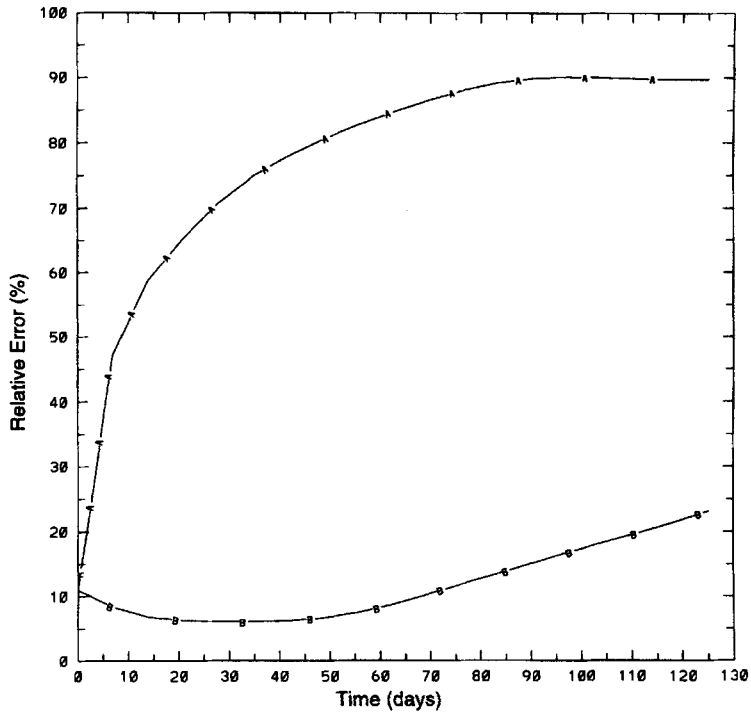

Figure 17(a). Baroclinic vortex; relative error for $E_c = u^2 + v^2$ on Ω_H. A. Monodomain on Ω_H: ξ_H^n. B. DM, $d = 0$: $\xi_H^{1,n}$

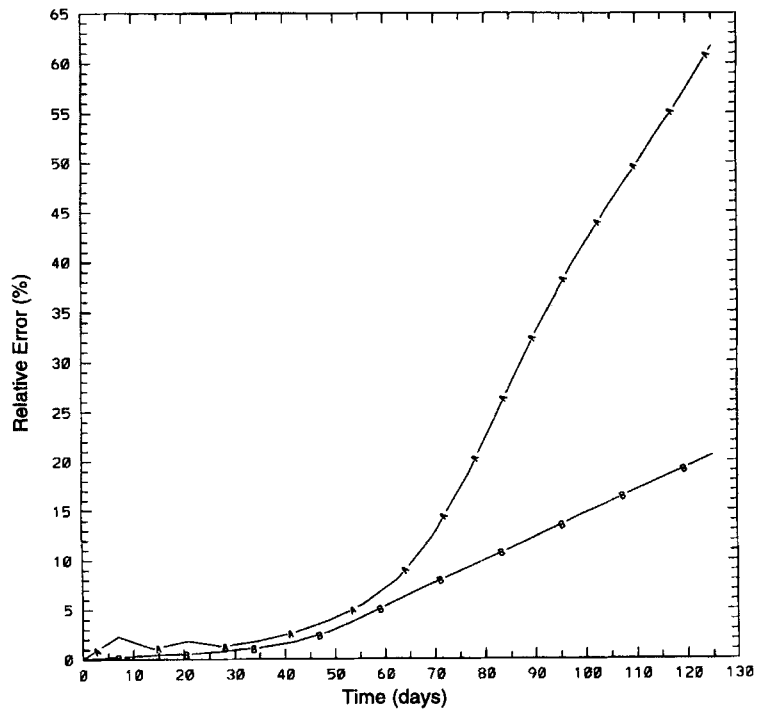

Figure 17(b). Baroclinic vortex; relative error for $E_c = u^2 + v^2$ on ω_h. A. Passive nested grid model: $\xi_h^{0,n}$. B. DM, $d = 0$: $\xi_h^{1,n}$

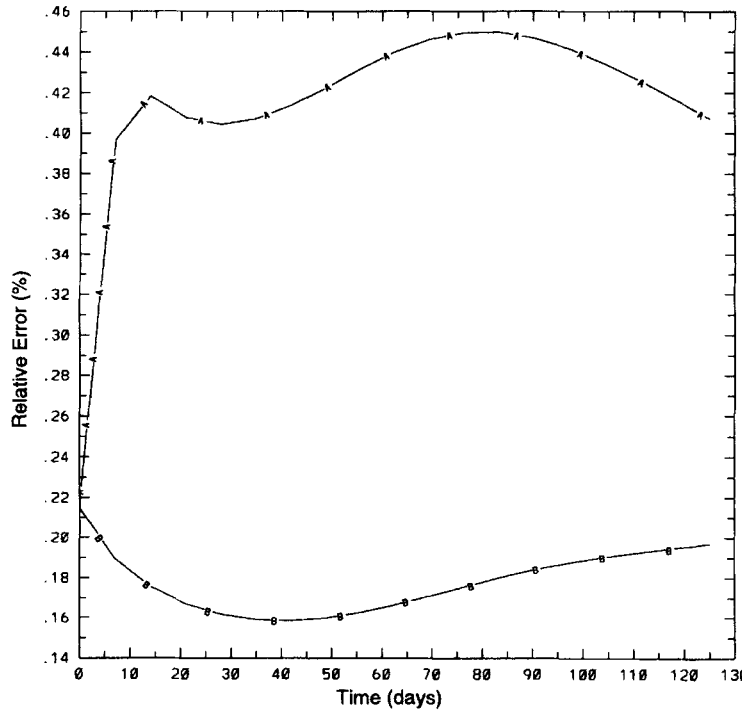

Figure 18(a). Baroclinic vortex; relative error for ρ on Ω_H. A. Monodomain on Ω_H: ξ_H^n. B. DM, $d = 0$: $\xi_H^{1,n}$

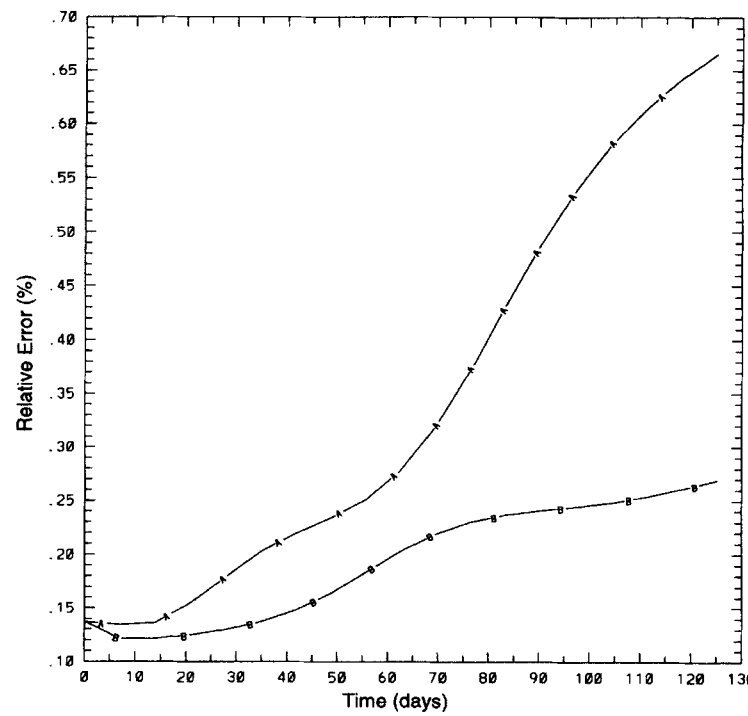

Figure 18(b) Baroclinic vortex; relative error for ρ on ω_h. A. Passive nested grid model: $\xi_h^{0,n}$. B. DM, $d = 0$: $\xi_h^{1,n}$

error before diverging. The same behaviour appears for the other methods for $d \neq 0$. Hence we have taken the value $d = 0$ for all other comparisons. In contrast with the case of the barotropic modon, the choice of d is here more critical. The optimal value of d is mainly dependent on the physics of the problem to be solved. In the case of the modon the solution depends essentially on the maximal barotropic tendency located at the centre. In this case the solution propagates without deformation of the initial structure. For the vortex the simulation is carried out in a stratified ocean and thus there are a large number of internal gravity waves which do not appear in the case of the modon. The quality of the interface boundary conditions is then essential for these waves to propagate correctly outside the local domain. If the distance d between the boundaries of the local domain ω and the correction domain $\tilde{\omega}$ is too large, the global solution near the local boundary is not sufficiently affected by the zoom correction, so the interactive nature of the nested grid model breaks down rapidly and finally the resulting solution diverges.

In contrast with the barotropic modon results, an increase in the parameter K from $K = 1$ to 2 improves both the coarse and the fine grid streamfunction solutions. In Figures 21 and 22 we have represented the relative error for Ψ on the CG with zoom for $K = 1$ and 2 for LDC and FIC methods respectively. For the two iterative methods the error found for more than two zoom iterations at each time step is not represented, because the optimal correction is obtained with $K = 2$. The cost in CPU time for two iterations of the LDC and FIC algorithms is approximately 20% more than with the DM (Table II).

For the three methods we have represented the error for the optimal streamfunction solution on the CG and FG in Figures 23(a) and 23(b) respectively. As a result of internal waves reflected at the solid boundaries of the global ocean domain propagating back into the zoom region and interacting with

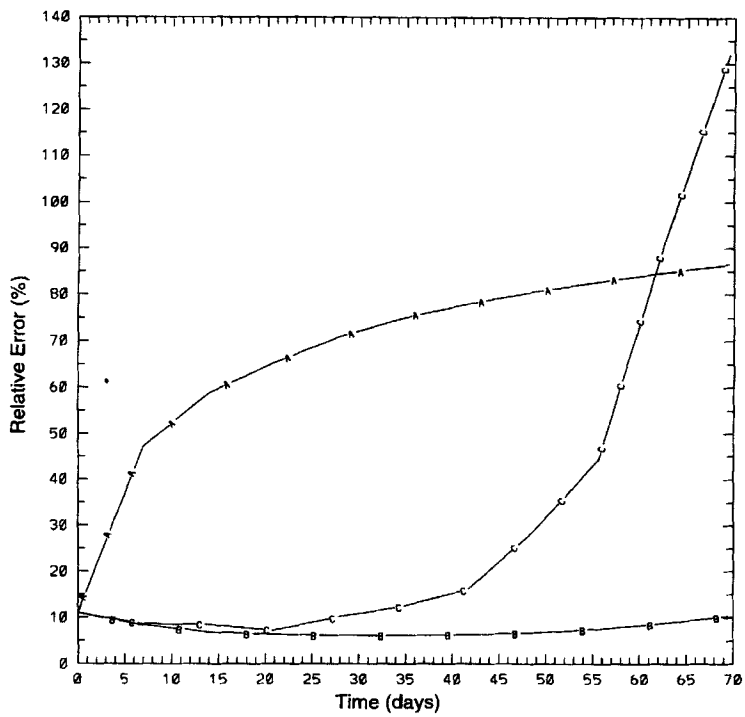

Figure 19. Baroclinic vortex; relative error for $E_C = u^2 + v^2$ on Ω_H. A. Monodomain on Ω_H: ξ_H^n. B. DM, $d = 0$: $\xi_H^{1,n}$. C. DM, $d = H$: $\xi_H^{1,n}$

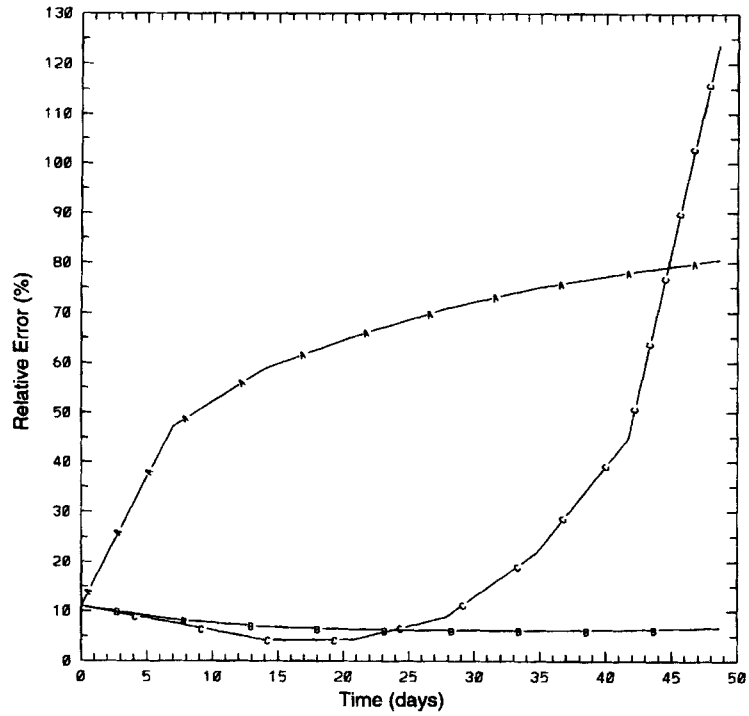

Figure 20. Baroclinic vortex; relative error for $E_C = u^2 + v^2$ on Ω_H. A. Monodomain on Ω_H: ξ_H^n. B. DM, $d = 0$: $\xi_H^{1,n}$. C. DM, $d = 2H$: $\xi_H^{1,n}$

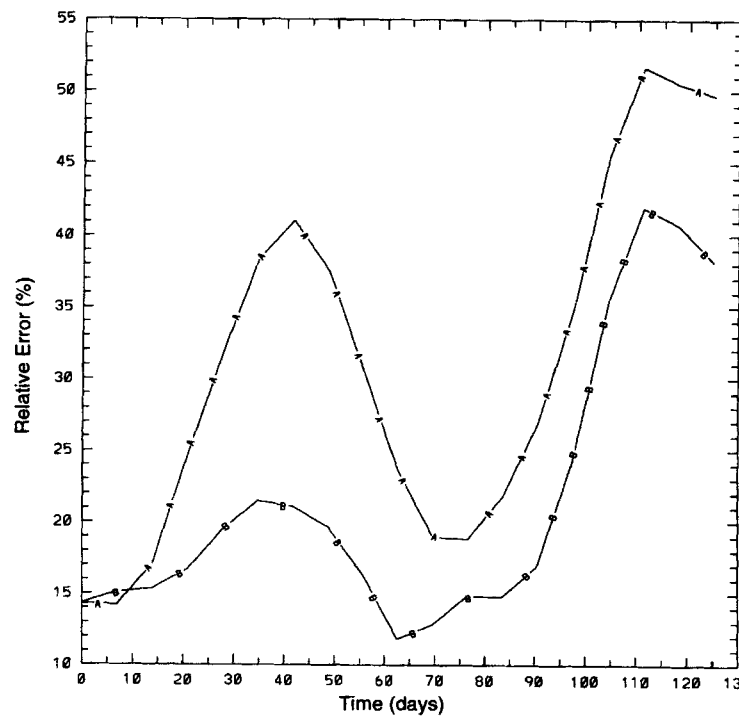

Figure 21. Baroclinic vortex; relative error for Ψ on Ω_H. A. LDC, $K = 1, d = 0$: $\zeta_H^{1,n}$. B. LDC, $K = 2, d = 0$: $\zeta_H^{2,n}$

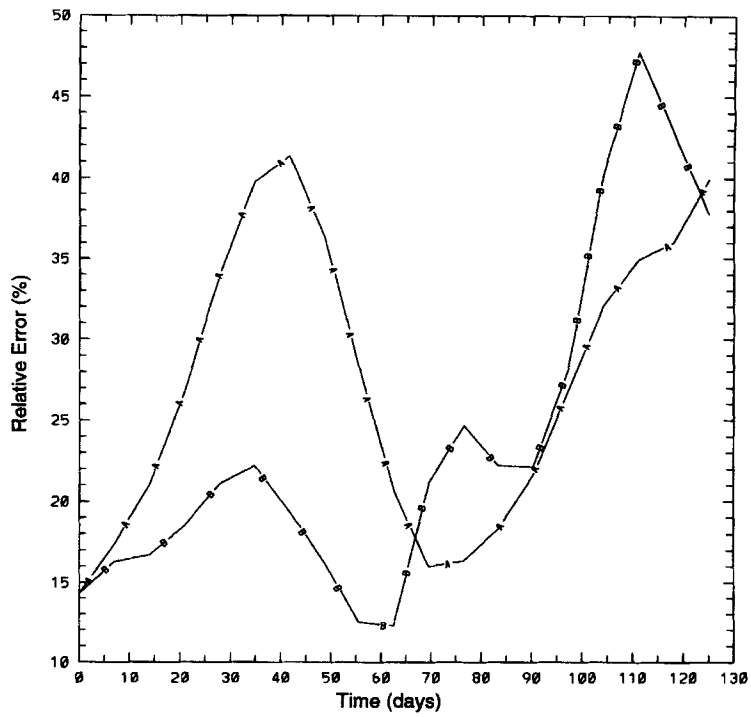

Figure 22. Baroclinic vortex; relative error for Ψ on Ω_H. A. FIC, $K = 1, d = 0$: $\xi_H^{1,n}$. B. FIC, $K = 2, d = 0$: $\xi_H^{2,n}$

the wake pattern, the errors are highly oscillating with time. The too weak horizontal resolution of the coarse grid does not allow us to accurately solve for the structure and phase speed of these waves developing outside the fine local grid. For the fine and coarse grid solutions until the 100th day the error curves B and C for the FIC and LDC solutions respectively are always below the curve A of the DM. After this date and until the end for the coarse grid solution the curve A is below the curves B and C. For the fine grid solution the same behaviour occurs until the 115th day. After this date the curves B and C come back below the curve A. The optimal solution is found with the LDC: the curve C is almost always below the other curves. If we compute the temporal average of the error, we get respectively 25·5%, 24% and 21·7% for the DM, FIC and LDC on the CG and 9·3%, 8·9% and 7·2% on the FG. We think that the solution obtained with the FIC or LDC is better than the one obtained with the DM because the two-domain solution depends on the quality of the interface boundary conditions for the local solution. Effectively, the direct method only calculates the correction term for (P_Ω) from the local second member $(G_z)_h$, whereas the iterative methods use the zoom correction directly evaluated from the local solution $(\Psi_t)_h$ for deriving implicitly appropriate interface boundary conditions for the local subproblem (P_ω). Moreover, the global and thus the local solutions are here corrected twice at each time step with two iterations of the local grid correction algorithm, which we cannot do with the DM. It is also important to notice that the zoom correction is, of course, really interesting and impressive as long as the currents of the vortex outside the fine local grid are not so important, i.e. until the 65th day. However, we have carried out the computations further in order to demonstrate the robustness of the zoom algorithms when the vortex crosses the grid interface.

For a more precise analysis, especially after the first 60–80 days, when the solution outside the local domain becomes quite complex (Figure 16), the influence of a finer coarse mesh on the global

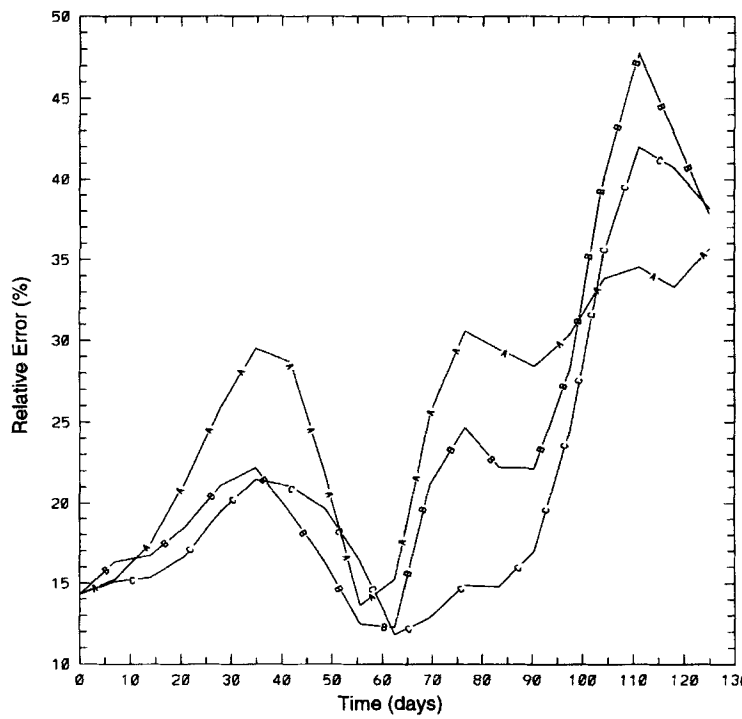

Figure 23(a). Baroclinic vortex; relative error for Ψ on Ω_H. A. DM, $d = 0$: $\xi_H^{1,n}$. B. FIC, $K = 2, d = 0$: $\xi_H^{2,n}$. C. LDC, $K = 2, d = 0$: $\xi_H^{2,n}$

domain Ω_H, as well as the influence of the relative size and position of the local domain ω, should be investigated.

It is also interesting to verify whether the vortex propagation at a larger Rossby number can be correctly described by the nested grid model. For that reason we have performed a similar simulation by increasing only the elevation height of the pycnocline to the value of 60 m, which indices an initial Rossby number $Ro = 0 \cdot 5$. In this case the propagation speed is higher and at the time $t = 125$ days the vortex is half outside the local domain. Nevertheless, during the crossing of the interface, no significant distortion of the vortex structure was observed (Figure 15(d)) as for the modon problem (Figure 3).

4.4. Discussion

The main purpose of this study was to compare three local grid correction methods for the resolution of the barotropic part, namely two iterative methods, FIC[10,11] and LDC,[12] and one direct method, DM.[6] This study is particularly interesting because the iterative methods LDC and FIC have not yet been tested much for such coupled problems. For more classical elliptic problems, convergence proofs can be established, but numerical experiments are absolutely required for complicated coupled problems such as those tested here. A first observation is that the iterative methods are a little more difficult to implement than the direct one, in particular the FIC which has been adapted in References 14 and 15 for the nested primitive equation model.

The three methods are compared on two test problems, proposed by Spall and Holland,[6] which are relevant to oceanic phenomena: a barotropic modon and a baroclinic vortex. The results indicate that

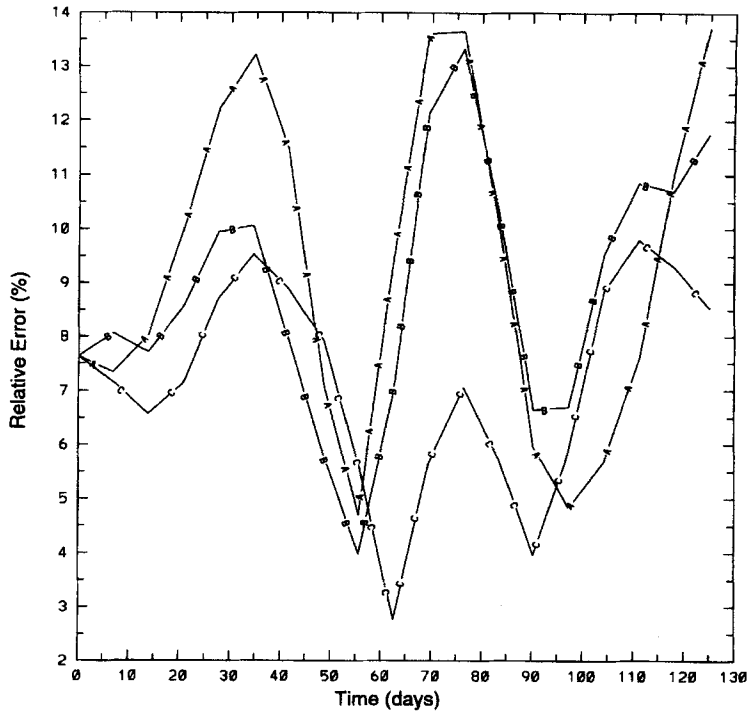

Figure 23(b). Baroclinic vortex; relative error for Ψ on ω_h. A. DM, $d = 0$: $\xi_h^{1,n}$. B. FIC, $K = 2, d = 0$: $\xi_h^{2,n}$. C. LDC, $K = 2, d = 0$: $\xi_h^{2,n}$

the interactive nested model allows us to manage efficiently in an implicit way the open outflow boundary conditions for the local grid resolution, which can therefore correct in a very good way the global solution by feedback of the local solution. We have then demonstrated the great efficiency of the interactive nested grid models in terms of gain in precision compared with the required CPU time. It appears that, essentially in the baroclinic case, the distance d which separates the local domain and the correction domain has a great influence upon the quality of the correction. In order to maximize the transmission of information from the local grid, the value chosen for d must be small enough, particularly for the coarse grid nodes which are used for the specification of the conditions for the open boundary of the local domain. The optimal value of d was found to be the same for the three methods in each test problem, namely $d = H$ for the modon and $d = 0$ for the vortex, and it was determined in an empirical way thanks to the numerical experiments.

In the case of the modon the computation of errors relative to the analytic solution shows that the three local grid correction methods yield approximately the same results for one iteration per time step of the iterative algorithm FIC or LDC. Hence we can think that DM is the optimal techniques because of its lower cost, but the results found in the case of the vortex indicate that it is not so easy to choose an optimal correction method for any problem of oceanic phenomena. Effectively, with the use of iterative methods only for the barotropic part, we find a nice improvement in the global two-domain solution in the case of the baroclinic vortex. Globally the LDC seems to be the best performing method despite its lack of conservation property, followed by the FIC and DM. However, these results are obtained with two iterations per time step of the local grid correction algorithm LDC

or FIC, which demands a little more CPU time than the direct method. The differences found between the two test problems are surely due to the physics of these phenomena. For example, in the two-dimensional case of the barotropic modon there are no important internal gravity waves present as there are in the case of the baroclinic vortex.

5. CONCLUSIONS

If we want to describe with a fine resolution of a numerical model the circulation in a local region of an ocean or a sea, such as a coastal zone, it is not possible for reasons of computation cost to perform a simulation with a high resolution over the entire domain. Therefore fine grids are generally only used over the local domain of interest. The problem is that it is very difficult to accurately parametrize the interaction between the fluid flow within the local domain and the surrounding fluid in the vicinity of the open outflow boundary. Various approaches exist to overcome this difficulty, as the use of radiation boundary conditions[21] or assimilation of observation data with the adjoint method.[22]

In this study we have presented a different approach using an interactive nested grid primitive equation model with local mesh refinement developed in References 1 and 2. Three correction methods (FIC, LDC and DM) have been incorporated for multigrid local mesh refinement into the numerical model OPA. The resulting numerical model was applied to simulate two oceanic phenomena: a barotropic modon with an analytical solution and a baroclinic vortex with a reference solution (obtained with a single fine grid over the entire domain). The results computed using the different correction methods were compared against the analytical and reference solutions and among themselves. The three methods were found to have similar accuracy for the case of the modon, whereas the two iterative methods (FIC and LDC) were found to be better than the DM for the case of the baroclinic vortex.

Our experience with the elliptic operator is encouraging, but we cannot make a general conclusion on the nested method. Moreover, some problems are still not resolved; for example, for baroclinic experiments the conservation of momentum, heat or salinity fluxes at the interface between the two embedded domains should be investigated more precisely.[15] Actually, whatever the local grid correction method used for the barotropic part, the nested technique that we have adopted does not allow us to conserve these quantities. Finally, note that the local grid correction methods have been tested here on academic problems without variable topography (constant $\mathscr{H}$). A situation with variable topography will be dealt with in our next work, consisting of a schematic study of the circulation in the Gulf of Lion.[2]

ACKNOWLEDGEMENTS

The authors would like to thank P. Delecluse for providing us with the code OPA. Supercomputer CPU time was provided by the Region Provence Alpes Côtes d'Azur on the CRAY YMP-2E of the Computing Center at the 'Institut Méditerranéen de Technologie de Marseille'.

REFERENCES

1. M. Laugier, L. Mortier and I. Dekeyser, 'Un Modèle bidomaine aux équations primitives en océanographie physique', *Oceanol. Acta*, **17**, 355–367 (1994).
2. M. Laugier, 'Développement d'un modèle multidomaine aux équations primitives pour des applications océaniques', *Thèse de Doctorat*, Université d'Aix-Marseille II, 1995 (unpublished).
3. G. W. Ley and R. L. Elsberry, 'Forecast of typhoon Irma using a nested-grid model', *Mon. Weather Rev.*, **104**, 1154–1161 (1976).

4. Y. G. Kurihara, G. J. Tripoli and M. A. Bender, 'Design of a movable nested-mesh primitive equation model', *Mon. Weather Rev.*, **107**, 239–249 (1979).
5. A. I. Falkovich, 'Nested grid scheme for predicting isolated vortex movement in a barotropic model of the atmosphere', *Sov. Meteorol. Hydrol.*, **9**, 35–41 (1986).
6. M. A. Spall and R. H. Holland, 'A nested primitive equation model for oceanic applications', *J. Phys. Oceanogr.*, **21**, 205–220 (1991).
7. L.-Y. Oey and P. Chen, 'A nested-grid ocean model: with application to the simulation of meanders and eddies in the Norwegian coastal current', *J. Geophys. Res.*, **97**, 20,063–20,086 (1992).
8. P. Delecluse, G. Madec, M. Imbard and C. Levy, 'OPA version 7: ocean general circulation model, reference manual', *Internal Rep. LODYC 9305*, 1993.
9. K. Bryan, 'A numerical method for the study of the circulation of the world ocean', *J. Comput. Phys.*, **4**, 347–379 (1969).
10. Ph, Angot, J. P. Caltagirone and K. Khadra, 'Une méthode adaptative de raffinement local: la correction du flux à l'interface', *C. R. Acad. Sci. Paris*, **315**, Sér. I, 739–745 (1992).
11. K. Khadra, Ph. Angot and J. P. Caltagirone, 'A comparison of locally adaptive multigrid methods: L.D.C., F.A.C. and F.I.C.', *NASA Conf. Publ. CP-3224*, 1993, Vol. 1, pp. 275–292.
12. W. Hackbusch, 'Local defect correction and domain decomposition techniques', in *Defect Correction Methods: Theory and Applications, Computing Supplement 5*, Springer, Vienna, 1984, pp. 89–1136.
13. W. Hackbusch, *Multi-grid Methods and Applications*, SCM Vol. 4, Springer, Berlin, 1985.
14. Ph. Angot and M. Laugier, 'La méthode FIC de raccordement conservatif de sous-domaines emboîtés pour un modèle de circulation océanique', *C. R. Acad. Sci. Paris*, **319**, Sér. II, 993–1000 (1994).
15. Ph. Angot and M. Laugier, 'Conservative matching of non-conforming grids with the nested multi-level zoom F.I.C. method; application to an ocean circulation model', *J. Comput. Phys.*, (submitted).
16. A. Arakawa and V. R. Lamb, 'Computational design of the basic dynamical processes of the UCLA general circulation model', *Methods Comput. Phys.*, **17**, 174–265 (1977).
17. R. Asselin, 'Frequency filters for time integration', *Mon. Weather Rev.*, **100**, 487–490 (1972).
18. G. Madec, C. Rahier and M. Chartier, 'A comparison of two-dimensional elliptic solvers for the streamfunction in a multilevel OGCM', *Ocean Model.*, **78**, 1–6 (1988).
19. G. R. Flierl, V. D. Larichev, J. C. McWilliams and G. M. Reznik, 'The dynamics of baroclinic and barotropic solitary eddies', *Dyn. Atmos, Oceans*, **5**, 1–41 (1980).
20. J. C. McWilliams, G. R. Flierl, V. D. Larichev and G. M. Reznik, 'Numerical studies of barotropic modons', *Dyn. Atmos. Oceans*, **5**, 219–238 (1981).
21. I. Orlanski, 'A simple boundary condition for unbounded hyperbolic flows' *J. Comput. Phys.*, **21**, 251–269 (1976).
22. U. Seiler, 'Estimation of open boundary conditions with the adjoint method', *J. Geophys. Res.*, **98**, 22,855–22,870 (1993)